2009

Mission analysis using experimental results from an 8-cm ion thruster

Andre A. Turner Jr.

MISSION ANALYSIS USING EXPERIMENTAL RESULTS FROM AN 8-CM ION THRUSTER

by

ANDRE A. TURNER, JR.

A THESIS

Submitted in partial fulfillment of the requirements
for the degree of Master of Science in Engineering
in
The Department of Mechanical & Aerospace Engineering
to
The School of Graduate Studies
of
The University of Alabama in Huntsville

HUNTSVILLE, ALABAMA

2009

In presenting this thesis in partial fulfillment of the requirements for a master's degree from The University of Alabama in Huntsville, I agree that the Library of this University shall make it freely available for inspection. I further agree that permission for extensive copying for scholarly purposes may be granted by my advisor or, in his absence, by the Chair of the Department or the Dean of the School of Graduate Studies. It is also understood that due recognition shall be given to me and to The University of Alabama in Huntsville in any scholarly use which may be made of any material in this thesis.

(student signature) 3/12/09 (date)

THESIS APPROVAL FORM

Submitted by Andre A. Turner, Jr. in partial fulfillment of the requirements for the degree of Master of Science in Engineering and accepted on behalf of the Faculty of the School of Graduate Studies by the thesis committee.

We, the undersigned members of the Graduate Faculty of The University of Alabama in Huntsville, certify that we have advised and/or supervised the candidate on the work described in this thesis. We further certify that we have reviewed the thesis manuscript and approve it in partial fulfillment of the requirements for the degree of the Master of Science in Engineering.

3/11/09 Committee Chair
(Date)

3-11-09

3-12-09

3/12/09 Department Chair

College Dean

5/4/09 Graduate Dean

ABSTRACT

The School of Graduate Studies

The University of Alabama in Huntsville

Degree Master of Science in Engineering College/Dept. Engineering/Mechanical and Aerospace Engineering

Name of Candidate Andre A. Turner, Jr.

Title Mission Analysis using Experimental Results from an 8-cm Ion Thruster

Ion thrusters are a type of electric propulsion device in which positively charged particles are electrostatically accelerated to create thrust. Ion thrusters are currently used for station keeping and deep space missions because of their high efficiency and specific impulse. This efficiency is a function of its beam voltage.

The effects of beam voltage on thrust, efficiency, and beam divergence were studied using experimental data from an 8-cm ion thruster. The beam voltage was varied between 600 V and 1400 V. Using these data, a mission analysis was performed for Lower Earth Orbit (LEO) to Mars and LEO to Jupiter.

Upper and lower bounds on beam divergence efficiency were calculated using experimental measurements of the plume expansion. Overall thruster efficiency increased monotonically with beam voltage. These performance data were input into CHEBYTOP to calculate trip time and propellant fraction for both the Mars and Jupiter missions. Trip time decreased with beam voltage while propellant fraction increased. Beam divergence was found to have a negligible effect on mission performance.

Abstract Approval: Committee Chair

Department Chair

Graduate Dean

ACKNOWLEDGEMENTS

Thanks to my advisors, Dr. Jason Cassibry and Dr. Zhongmin Li, and committee members, Dr. Georgia Richardson and Dr. Robert Adams, for all the advice, support, and persistence in assuring the completion and quality of this project. My acknowledgements also go out the Propulsion Research Center and its former director, the late Dr. Clark Hawk, and to the Bridge to the Doctorate Fellowship Program and its principal investigator for both providing facilities and resources for me during this endeavor.

Thanks also to my family, especially my dad, mom, and Mama, for being a constant source of encouragement and support among other things. And to all the rest of my family and friends for keeping happy and grounded, thanks always.

TABLE OF CONTENTS

PAGE

LIST OF FIGURES

FIGURE **PAGE**

LIST OF TABLES

TABLE **PAGE**

LIST OF ACRONYMS

DAQ	Data acquisition system
DC	Direct current
DCIU	Digital control and interface unit
ETS	Engineering Test Satellite
EP	Electric propulsion
LEO	Lower earth orbit
MFC	Mass flow controller
NSSK	North-south station keeping
NSTAR	NASA Solar Electric Propulsion Technology Applications Readiness
PPS	Probe positioning system
PPU	Power processing unit
PRC	Propulsion Research Center
SERT	Space Electric Rocket Test
XIPS	Xenon Ion Propulsion System

LIST OF SYMBOLS

A	Neutral atom
A^+	Ion
A_p	Surface area of the collecting probe
B	Buffer size
D	Source diameter
e^-, e_A^-	Electron
$\tilde{e}^-$	High energy electron
g_0	Gravitational constant
I_A	Accelerator grid current
I_B	Beam current
I_D	Discharge current
I_F	Filament current
I_{sp}	Specific impulse
I_t	Total impulse
I_{sp}	Specific impulse
I_t	Total impulse
in	Inches
J	Current
j	Current density
k	Solar gravitational constant
kg	Kilograms
kW	KiloWatts
M	Molecular weight of Argon
mA	MilliAmps
m_f	Final weight of the propulsion system
m_0	Initial weight of the propulsion system
m_{pp}	Mass of the power plant
$\dot{m}$	Mass flow rate of the propellant
$\dot{m}_{Ar}$	Mass flow rate of Argon
$\dot{m}_{ion}$	Ion mass flow rate
P_A	Accelerator grid power
P_B	Beam power
P_D	Discharge power
P_F	Filament power
P_e	Converted electrical output
P_{ion}	Ionization power
$P_{thruster}$	Thruster power
P_{total}	Total power
P_{util}	Utilization power
R	Probe circuit resistance
S	Sample rate
S_τ	Flight distance at constant burn
s	Seconds
T, τ	Trip time
T_A	Acquisition time
T_D	Delay time
T_{ion}	Thrust produced by the ion thruster
t_b	Burn time
$t_{\%}$	Coverage factor
V	Voltage drop/ volts
V_A	Accelerator grid voltage
V_B	Screen grid voltage (beam voltage)
V_D	Discharge voltage
V_F	Filament voltage
v_t	Translational velocity
v_e	Exhaust velocity
U	Uncertainty
u_c	Combined Uncertainty
x_n, x_{n+1}	Divergence distance
x_a	Distance between the accelerator grids
x_{peak}	Sweep position at peak of sweep profile
$x_{10\%left}$	Left sweep position at 10 % peak

$x_{10\%right}$	Right sweep position at 10 % peak
$x(t)$, r	Position vector
y_n, y_{n+1}	Distance from the source
α	Specific mass/power
γ	Payload mass fraction
Δv	Velocity increment
ε	Permittivity of free space
$\eta_{overall}$	Overall efficiency
η_{PPU}	Power processing unit efficiency
$\eta_{thruster}$	Thruster efficiency
η_{util}	Mass utilization efficiency
θ	Divergence angle

CHAPTER 1

INTRODUCTION

The interest in electric propulsion (EP) systems comes as a result of their relatively high efficiency of propellant mass use (Jahn 1996) when compared with chemical propulsion. An EP system is a set of components which converts electrical power from the spacecraft power system into the kinetic energy of the propellant (Martinez-Sanchez and Pollard 1998). In the case of electrostatic and electromagnetic systems, the propellant is accelerated directly by electromagnetic body forces, resulting in very high exhaust velocities (~10^4 to 10^5 m/s). This corresponds to an increase in propellant fraction for longer space missions in accordance with (Jahn 1996)

$$\frac{m_f}{m_0} = e^{-\Delta v/v_e}, \tag{1.1}$$

where m_f / m_0 is the payload fraction with m_f and m_0 being the final and initial weight of the propulsion system, respectively, v_e is the exhaust velocity, and Δv is the velocity increment achieved by ejection the necessary propellant.

Out of convenience, we define the *specific impulse*, I_{sp}, as the total impulse per unit weight of propellant (Sutton and Biblarz 2001),

$$I_{sp} = I_t / (\dot{m} g_0) = v_e / g_0, \tag{1.2}$$

where I_t is the total impulse, $\dot{m}$ is the mass flow rate of the propellant, and g_0 is the gravitational constant. Consequently, the specific impulse plays an important role in long missions or missions with large Δv requirements. A comparison of specific impulse for various propulsion systems is given in Table 1.1. In this table, $\eta_{thruster}$ is the thruster efficiency, and $\dot{m}$ is the mass flow rate of the propellant.

Table 1.1 Typical performance values (Sutton and Biblarz 2001)

Engine Type	$\eta_{thruster}$	I_{sp} (s)	v_e (m/s)	$\dot{m}$ (kg/sec)	Power Input (kW)
Chemical rocket	0.50	300	2940	0.0340	294
Nuclear Fission	0.50	800	7840	0.0128	787
Arc-electrothermal	0.50	600	5880	0.0170	588
Ion electrotstatic	0.90	2000	19600	0.0051	1959

While propellant fractions can be quite high for many types of EP missions, all EP systems are power limited, which leads to low thrust levels and consequently longer burn times to achieve the desired acceleration. However, missions with large Δv in which flights can take months, the high I_{sp} permits long burn durations (>10000 hours) (Brophy 2002) and the high exhaust velocity enables high vehicle velocities and shorter trip times compared with chemical systems for some missions.

1.1. Ion Thrusters

EP systems are generally classified in one of three categories (Sutton and Biblarz 2001):

1. *Electrothermal.* Propellant is heated electrically and expanded thermodynamically, i.e., the gas is accelerated to supersonic speeds through a nozzle, as in the chemical rocket.

2. *Electrostatic.* Acceleration is achieved by the interaction of electrostatic fields on non-neutral or charged propellant particles such as atomic ions, droplets, or colloids.
3. *Electromagnetic.* Acceleration is achieved by the interaction of electric and magnetic fields within the plasma. Moderately dense plasmas are high-temperature or nonequilibrium gases, electrically neutral and reasonably good conductors of electricity.

The ion thruster, which is the focus of this thesis, is an EP system that accelerates charged particles electrostatically with the help of electrical grids. Ion thrusters work by injecting the propellant into an ionization chamber, where a hollow cathode or filament cathode emits electrons, and by way of electron bombardment, the neutral propellant is ionized. The positive ions are accelerated by the electric field between screen and accelerator grids, pass through the screen, and are propelled out of the thruster. The plume of ions is then combined with a neutralizing stream of electrons to produce a net charge of zero and thrust, shown in Figure 1.1 (NASA 2007).

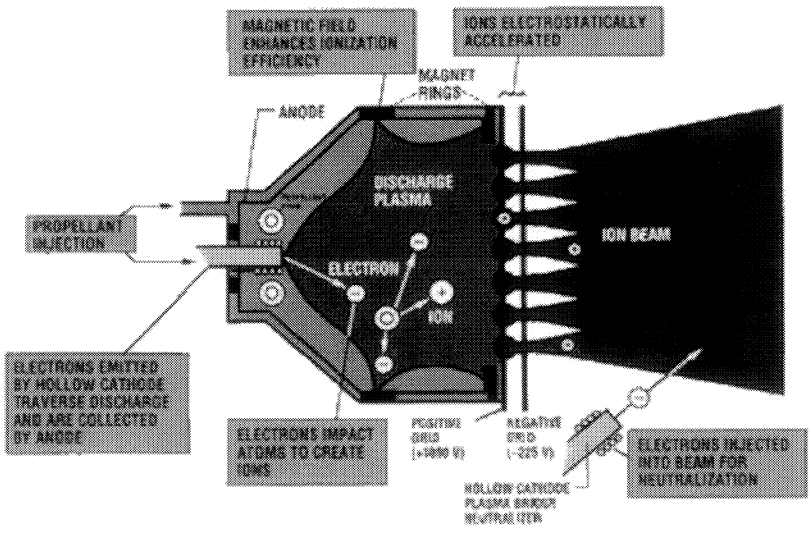

Figure 1.1 Ion thruster diagram (NASA 2007)

The ion thruster gets its name from the fact that the change in momentum is due to the acceleration of ions. Modern thrusters commonly utilize electron bombardment in the ionization process, in which a high energy electron, $\tilde{e}^-$, collides with a neutral atom, A, to produce an ion, A^+, and electrons, e_A^- and e^-, according to the inelastic collision (Jahn 1996),

$$\tilde{e}^- + A \Leftrightarrow A^+ + e_A^- + e^-, \tag{1.3}$$

where e_A^- does not necessarily have the same energy as e^-. The electrons are trapped by interactions with the internal magnetic and electrostatic fields. The latter accelerates the ions out of the ionization section. In the exhaust plume where the ions are neutralized by a separate electron stream, the thrust is derived almost entirely by the ion motion, since the ion mass is 10^3 to 10^4 times heavier than the electron (Sutton and Biblarz 2001). Furthermore, with use of ions rather than electrons as a means of momentum exchange, an emphasis is placed on the voltage potential rather than the current of the electron emitting cathodes. This aids in the simplicity of the power source because of the added wiring and switches associated with high currents.

With all types of EP, much of the importance is placed on the power source, or more specifically mass, conversion efficiency, and operation at low or high I_{sp} as related to the power source. The mass of the power plant (or source), which includes the thruster, propellant storage and the feed system, the energy source with its conversion system and auxiliaries, and the associated structure (Sutton and Biblarz 2001), is related to the conversion efficiency by way of the specific power α, which is defined as (Sutton and Biblarz 2001)

$$\alpha = P_e / m_{pp}, \tag{1.4}$$

where P_e is the converted electrical output and m_{pp} is the mass of the power plant. Currently, values of α range from 100 to 200 W/kg with near term technologies expected to reach 500 to 2000 W/kg (Sutton and Biblarz 2001).

Variations in beam voltage, which can be adjusted during operation, directly affect thrust, efficiency, and I_{sp}. The beam voltage is essentially the throttling mechanism for the ion thruster because it sets the electric potential between the screen and acceleration grids. The beam voltage, which is positive with respect to ground, is applied to the screen grid and a negative voltage is applied the accelerator grid resulting in an electric potential between the two grids.

Major considerations have to be made concerning the power sources (e.g., solar and nuclear power sources), whereas most of that power required to operate an ion thruster goes to the beam voltage (Foster, et al. 2004), and its mass and power output as it relates to the beam voltage. Additionally, this power has to be processed, controlled, and distributed so the power processing unit (PPU) mass and capabilities have to be considered when operating an ion thruster. A solar power source is ideal when in close proximity and properly orientated to the sun. For missions with large times spent in the shadow of planets or moons, or missions to the outer planets, onboard power must be supplied. The currently available options include nuclear, batteries, and fuel cells. Beam voltage, beam current, and propellant flow rate are among the parameters that are adjusted to optimize operation, reduce trips times, and increase payload knowing the power limitations and other constraints of a given mission.

1.2. Road Map to Thesis

Since beam voltage plays such a vital role in ion thruster operation, this thesis focuses on the effects its variation has on vehicle performance parameters during two different missions: lower earth orbit (LEO) to Mars orbit transfer and LEO to Jupiter orbit transfer. Specifically, thrust, specific impulse, thruster efficiency, and overall efficiency were determined from measurements taken on an 8 cm ion thruster in which beam voltage was varied. The performance data were fed into computer models which calculate orbit trajectories, trip times, and propellant fraction. Since our 8 cm ion thruster is an experimental device not intended for space applications, the orbital trajectory calculations are qualitative but should reflect the basic trends of space-rated thrusters.

Chapter 2 presents a more detailed description of the ion thruster, early and modern applications, and previous research involving beam voltage. This chapter will also contain information about the different missions we have studied. Chapter 3 covers the experimental setup including the ion thruster, probes, data acquisition system, vacuum facility, and the probe positioning system. Data analysis and modeling are given in Chapter 4, which includes the description of analysis, test matrix and scope, and modeling of orbit trajectories. Chapters 5 and 6 give the results & discussion, and conclusions, respectively.

CHAPTER 2

BACKGROUND

There is a wealth of knowledge on the history of electric propulsion. Excellent reviews have been given by Goebel and Katz and Jahn in their books *Fundamentals of Electric Propulsion: Ion and Hall Thrusters* (Goebel and Katz 2008) and *Physics of Electric Propulsion* (Jahn 1996). For completeness, we will highlight relevant milestones (Choueiri 2004), while drawing heavily from existing sources. In particular, we will discuss ion thruster history, development, applications, and theory of operation. Proceeding historical developments, we will discuss the anatomy of modern ion thrusters (Goebel and Katz 2008), and discuss key physics issues (Jahn 1996).

Electric propulsion was first conceived by Robert Goddard in 1906 (Goddard 1960) as a means of manned propulsion, followed by an independent description by Tsiolkovsky (T. M. Mel'kumov 1964) in 1911.

Following the so-called era of the pioneers (Choueiri 2004), the first flight test on an ion thruster was on July 20, 1964, when the SERT I (Space Electric Rocket Test) with two ion thrusters attached on side (Jahn 1996). For several decades, primarily experimental flights were conducted by multiple countries, including the US, Japan, and Russia. One of the first operational ion thrusters was attempted in 1995 for north-south station keeping (NSSK) on a Japanese communications satellite Engineering Test

Satellite (ETS) VI (Shimada, Sato et al. 1987). The United States' first commercial use for NSSK of the thruster type was in 1997 with Hughes Xenon Ion Propulsion System (XIPS) (Beattie June 1998), and NASA utilized the Solar Electric Propulsion Technology Applications Readiness (NSTAR) in 1998 on Deep Space One (Brophy 2002). Following these successes in the late 1990's, there has been a growth of ion thruster applications to include drag compensation, attitude adjustment, interplanetary and deep space missions. There are also many more ion thrusters in development for commercial and government missions.

2.1. Anatomy of a Modern Ion Thruster

Modern ion thrusters used in current in-space propulsion generally have three main components: the ion source, the accelerator grids, and the neutralizer cathode, shown in Figure 1.1. The ions produced by the cathode are accelerated out of the thruster as result of the electric potential across the accelerator grids. The propellant is primarily positively charged ions, and this ion exhaust stream is neutralized by neutralizer cathode.

Ion generation in modern ion thrusters is usually accomplished by one of three distinct methods: direct current (DC) electron discharge, radio frequency, or microwave discharge. We will limit the discussion to DC electron discharge since it is the most popular approach, and is used in this research.

In DC electron discharge, an emitter filament or other material is electrically heated to emit electrons. Early electron bombardment ion thrusters developed in the 1960's utilized a heated tungsten filament for plasma discharge, with a smaller filament used as a neutralizer. However operation of these requires high heater power, on the

order of the discharge power, which substantially decreases the efficiency of the thruster (Goebel and Katz 2008). This problem was solved with the implementation of the hollow cathode. The hollow cathode as shown in Figure 2.1, is a hollow tube which has an electron emitting insert, which when heated, causes the electrons to ionize the propellant gas that flows through the tube. The result of this is a low potential plasma that is attracted out of the orifice plate for its ions to later be accelerated.

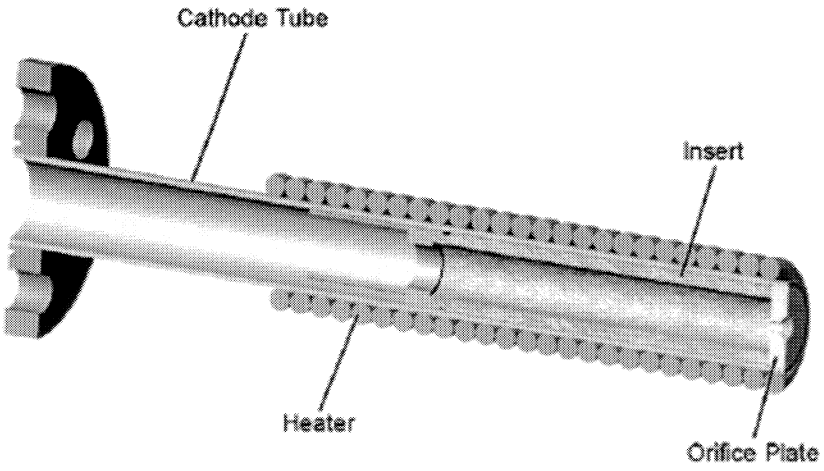

Figure 2.1 Hollow cathode (Goebel and Katz 2008)

When electrons are emitted by the cathode or hot filament, they are attracted to the anode because of its positive potential. This positive potential applied to the anode is called the discharge voltage, V_D. Adjustments in V_D will increase or decrease the electron energy of the ionizing (plasma creating) electrons. Although these electrons are attracted to the anode, they are not allowed to reach it because of an externally applied weak axial magnetic field, shown in Figure 2.2. These magnets cause the electrons to spiral axially back and forth in the discharge chamber until they bombard a propellant

atom (Jahn 1996). These magnets are generally permanent magnets, which means they have no need for extra power and they do not dissipate heat.

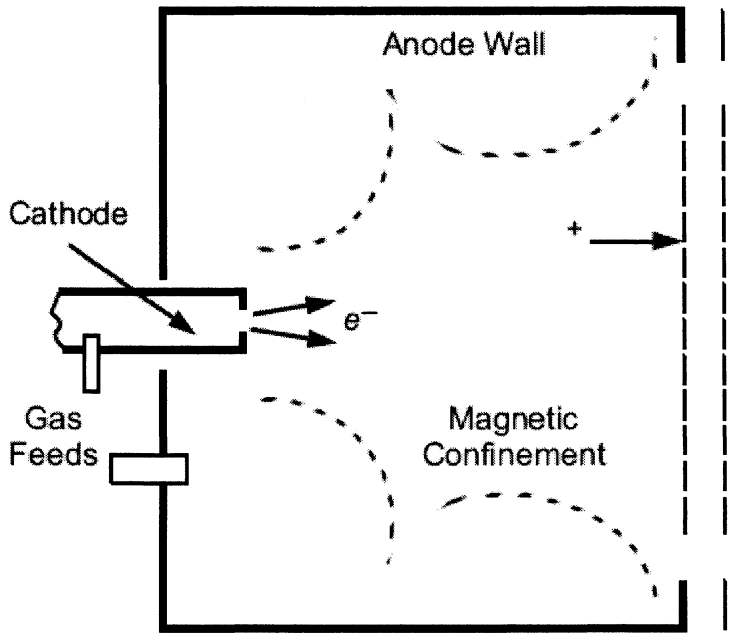

Figure 2.2 Discharge chamber with magnetic field (Goebel and Katz 2008)

The acceleration grids or ion optics serve three main purposes: to extract ions from the discharge chamber, to accelerate ions to produce thrust, and to prevent electron backstreaming (Goebel and Katz 2008). Ions born from electron bombardment at a potential higher than the screen grid's potential (beam voltage) drift towards the screen. The potential difference extracts them from the discharge chamber. This is where the terms ion optics and screen come from: the fact that as these ions leave the chamber, and the screen grid orientates and focuses the ion beamlets to reduce ionic impact on the

accelerator grid. The accelerator grid does more focusing and accelerates the ions to produce thrust as shown in Figure 2.3 from Jahn.

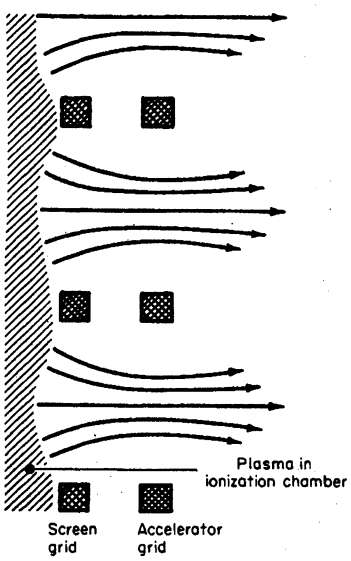

Figure 2.3 Ion beamlet focusing (Jahn 1996)

The accelerator grid also is set at a low enough potential to prevent the neutralizing electrons from backstreaming, which reduces the acceleration efficiency of the thruster. All of the electrical components on ion thrusters are powered by the power processing unit (PPU), which converts electrical energy from its solar arrays into current and voltages required to run the engine. The propellant feed system and the PPU are controlled by the Digital Control and Interface Unit (DCIU), which accepts and executes high-level commands from the spacecraft computer and provides propulsion subsystem telemetry to the spacecraft to the spacecraft data system (Noca 2001). A measure of the power processing capabilities of PPU per unit mass of the system is the specific power, α, as mentioned in Chapter 1.

2.2. Beam Voltage

Beam voltage is the voltage applied to the screen grid that sets the potential between the accelerator grids as seen in Figure 2.4. This potential causes the discharge of ions from the thruster which creates its thrust. One of the many ways to throttle an ion thruster is to adjust the beam power; this is done by adjusting the beam voltage and/or beam current (Rawlin 1995). Adjusting the beam power also affects thruster parameters such as exhaust velocity, specific impulse, efficiency, and erosion.

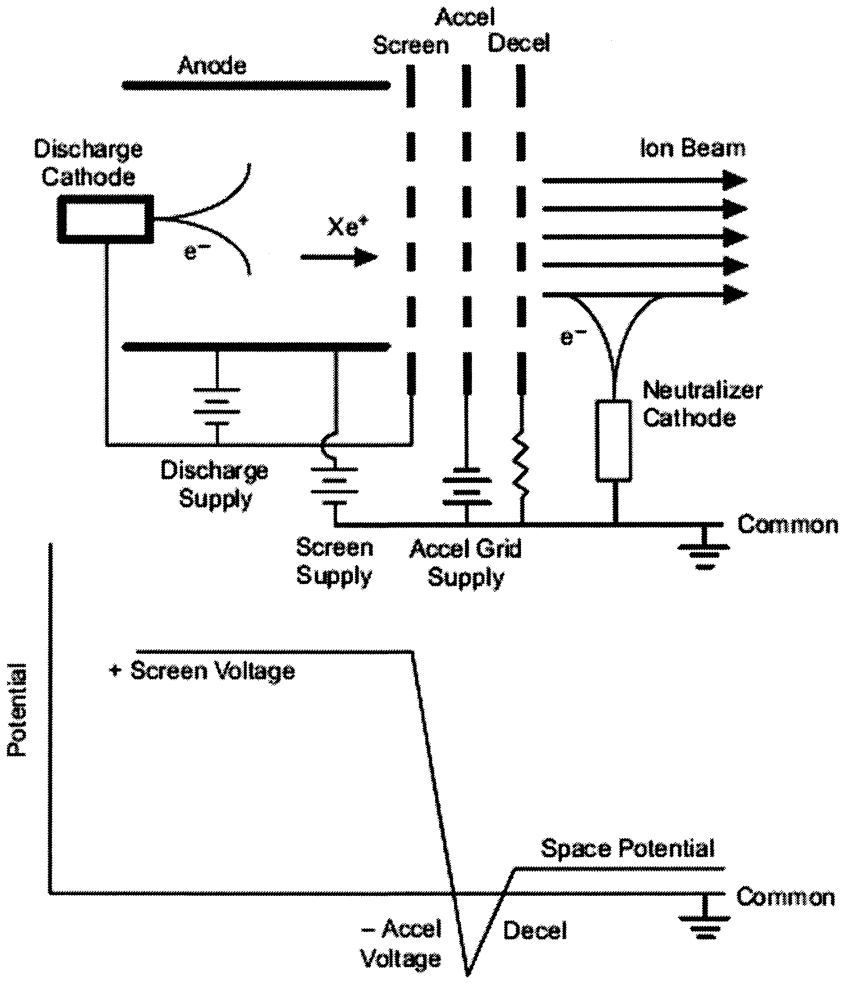

Figure 2.4 Ion thruster electric potential diagram (Goebel and Katz 2008)

The basic principle of the ion thruster is that ions are accelerated due to the electric potential between screen and accelerator grid. So, in theory, any change in beam voltage should affect the rate at which the ions leave the thruster. This does in fact happen as shown in equation 2.1 from (Jahn 1996),

$$v_e = \left(\frac{2qV_0}{M} \right)^{1/2}, \tag{2.1}$$

where v_e is exhaust velocity, q is electric charge, M is the molecular weight of the propellant gas, and $V_0 = V_B - V_A$ is the electric potential across the beam voltage of the screen grid (V_B) and the voltage of the accelerator grid (V_A). The specific impulse is directly affected since,

$$I_{sp} = \frac{v_e}{g_0}, \tag{2.2}$$

where g_0 is the gravitational constant.

There are limitations on beam voltage that keep its value from being raised to an infinitely high voltage to accelerate the ions. The first and most important is available power. Beam power consumes a vast majority of the total power of the thruster and any raises in that value have to be considered against power needs of other thruster components and limitations of the power source. Another limitation is electron backstreaming, which reduces efficiency if significant. If beam voltage is raised too high, it negates the accelerator's grid ability to repel electrons, because the electrons are attracted to the high positive voltage.

2.3. Mission Analysis

Because variations in beam voltage have such a major impact on specific impulse, thrust, and efficiency, these variations will also impact propellant fraction and trip time for missions. The purpose of this research is to measure effects that beam voltage has on operation of an 8-cm ion thruster, and estimate the impact on missions of interest. To do this, beam voltage was varied from 600 V to 1400 V, and thrust, specific impulse, efficiency, and beam divergence were determined from the experiments. To put this into context of a space application, two mission studies were performed to calculate

propellant fraction and trip time as a function of beam voltage, factoring in the thruster performance based on the experimental data. The two missions are an orbit transfer from LEO to Mars and LEO to Jupiter.

Thrust, specific impulse, and efficiency were calculated using readings from the thruster's PPU system that displays the voltages and currents of the hot filament cathode, discharge, accelerator grid, and screen grid. The beam divergence was found by doing a sweep of the thruster's plume at different distances from the thruster using Faraday probes. The results of the plume sweep were analyzed to determine divergence.

The mission analyses was done using the Chebytop (Polsgrove 2006) program for the Mars and Jupiter missions, using the results of calculations of thrust, specific impulse, and efficiency. Using the specific impulses calculated for each beam voltage and other inputs, and at constant specific mass (1/specific power), the propellant fraction and trip time as functions of beam voltage and specific impulse are calculated.

2.4. Summary

The ion thruster, first conceived for manned missions, has developed into a proven method for space propulsion. By accelerating positively charged particles using voltage potential, the thruster achieves very high exhaust velocities and efficiency, albeit low thrust. This is suitable for high Δv / low thrust missions. In the next chapter we will discuss our experimental ion thruster and the mission analysis program used to study the effects of beam voltage on propellant fraction and trip time for missions of interest.

CHAPTER 3

EXPERIMENTAL SETUP & DIAGNOSTICS

The experimental setup for the operation and diagnostics of the ion thruster consisted of the 8-cm diameter ion source, the vacuum facility, the power supply processing unit, argon gas supply, gas supply and mass flow controllers, Faraday probes, probe positioning system (PPS), and data acquisition system (DAQ), Figure 3.1. Power to the thruster is controlled externally by the PPU. Various propellants are fed and controlled by the mass flow controller (MFC). The probes are placed on the PPS and swept across the plume, and the data is captured by the DAQ system. Below we discuss the apparatus and procedures in detail. Section 3.1 describes the experiment and Section 3.2 discusses the diagnostics.

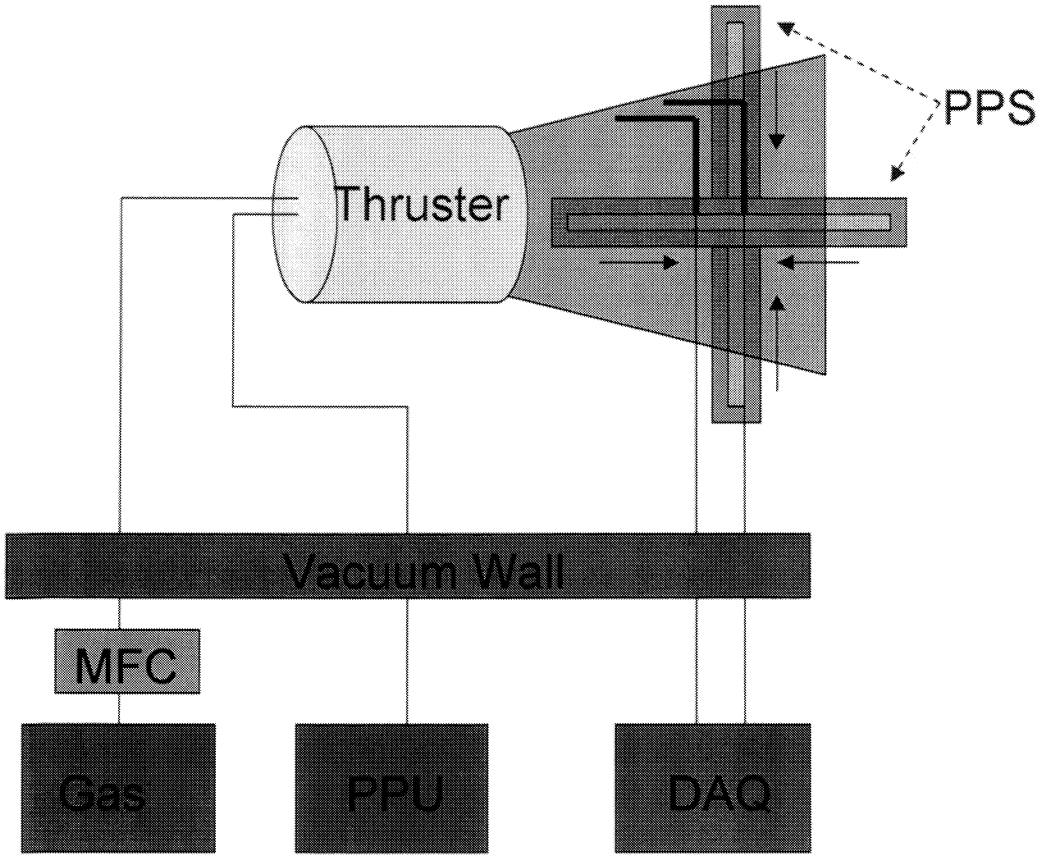

Figure 3.1 Ion thruster facility setup

3.1. Experimental Setup

The experiments were performed at The University of Alabama in Huntsville's (UAHuntsville) Propulsion Research Center (PRC) located within the Johnson Research Center. As shown in Figure 3.1, the setup consists of a vacuum facility, 8 cm ion source, gas supply and propellant feed control. Below we describe these subsystems in detail.

3.1.1. Vacuum Facility

To simulate space vacuum pressures, the ion thruster is operated inside of UAHuntsville's 1.8 m diameter (10.4 m^3) vacuum test facility, shown in Figure 3.2.

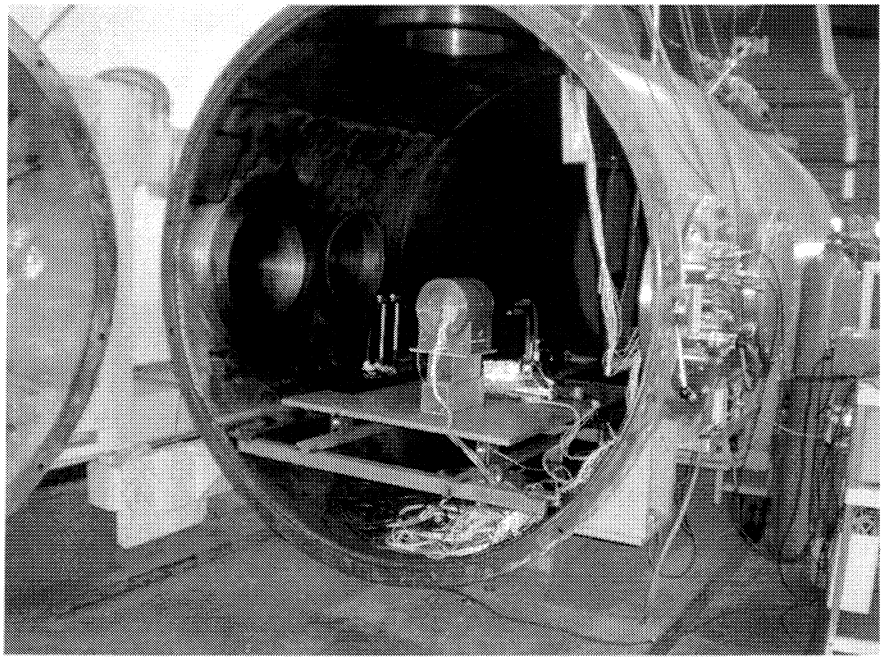

Figure 3.2 Ion thruster mounted in the UAHuntsville vacuum chamber

The chamber has an argon pumping speed of 10,000 l/s and maintained base vacuum pressures of about 2.5 x 10^{-5} Torr. To attain these capabilities, the vacuum facility has a Stokes Microvac 1 horsepower roughing pump, Duo Seal model 1397 foreline pump, and a CVC 20" diffusion pump.

3.1.2. Plasma Process Group (PPG) 8-cm Diameter Ion Source

The PPG 8-cm ion thruster, shown in Figure 3.3, was operated using argon gas as the propellant. The plasma source was a tungsten filament cathode and neutralized using a smaller filament neutralizer. The screen and accelerator grids have 913 circular aperture holes of 1.93 mm and 1.141 mm diameter, respectively. The grid material thickness is 1.524 mm and the screen grid has been thinned to 0.508 mm. The grid gap is 6 mm. The

source can be operated with beam energy from 50 to 1500 eV (Li, et al. 2005). The thruster was controller and powered by PPU MPS-5001 power processing unit.

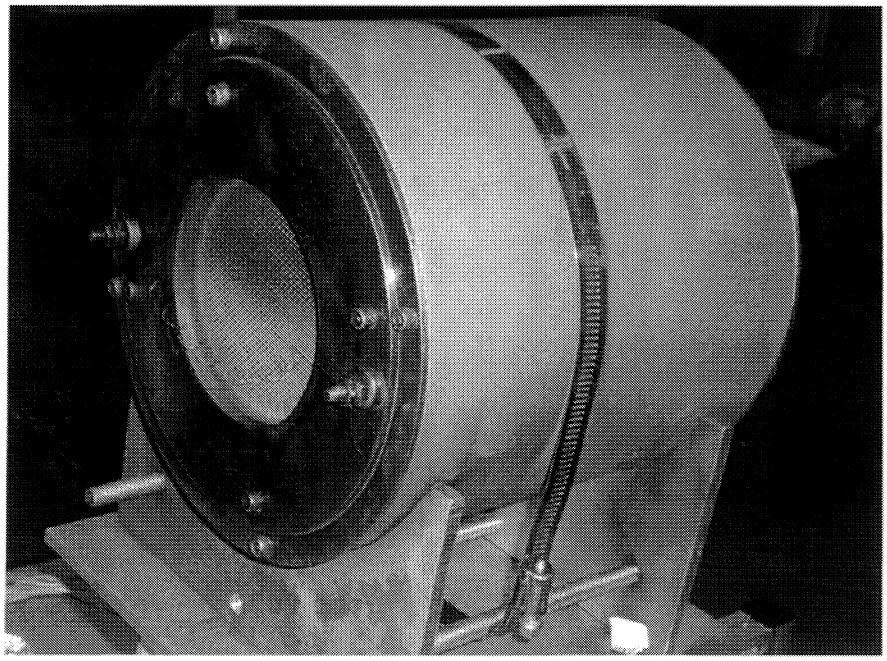

Figure 3.3 UAHuntsville's 8-cm ion thruster

3.1.3. Gas Supply and Mass Flow Control

Argon gas flow to the thruster comes from 99.999% purity argon tank supplied at 20 psi and feeds through the vacuum chamber wall. The gas flow from the tank is controlled by a MKS mass flow controller that can sustain max flow of 20 sccm. Similarly, the flow could be adjusted to the desired flow rate by the MKS 246 on the control panel.

3.2. Diagnostics

Various measurements were taken in order to calculate the thrust, specific impulse, and efficiency of our 8 cm ion thruster. Performance measurements were determined with readings from the PPU system, which displayed beam current and voltage, accelerator voltage, accelerator current and voltage, neutralizer emission current, filament current, discharge current and voltage, and neutralizer filament current. Analysis of data from the PPU system is discussed in Chapter 4.

A single plume diagnostic was required to measure beam divergence, and consisted of a pair of Faraday probes. Faraday probes measure ion current density, and were placed on a 2-D stepper motor actuator and swept across the plume at varying distances from the source. The probe sweep produced current density profiles that were captured on an oscilloscope and later analyzed in MathCAD.

Faraday probes capture ion current density by being biased negatively with respect to the plume, thus attracting the positively charged ions and repelling the negative ions. A Faraday probe consists of an inner collecting surface usually made of tungsten, a ceramic insulator, and an outer conducting ring, shown in Figure 3.4. The inner collecting surface is usually made of tungsten or other metal coated with tungsten to prevent secondary electron emission caused by the high energy ions colliding with collecting surface (Linnell and Gallimore 2006). The outer ring and sometimes the inner collecting surface are biased negative with respect to plasma, thus repelling electrons. The outer ring is usually made out stainless steel or some other metal. The ceramic insulator is used to shield the collecting surface from the negatively biased outer ring. Ions flowing to the collecting surface create a current which flows through a circuit

connected to the inner probe. From the voltage drop across a resistor in that circuit, shown in Figure 3.5, the current can be found from the relation:

$$V = JR, \tag{3.1}$$

where V is the voltage drop, J is the current, and is R the probe circuit resistance. The current density is a function of Faraday probe surface area and collected current and can be found from (Schuettpelz, et al. 9-12 July 2006)

$$j = \frac{J}{A_p}, \tag{3.2}$$

where j is current density and A_p is surface area of the collecting surface.

The Faraday probe configuration, shown in Figures 3.4 and 3.5, consisted of a 3/8" diameter tungsten rod collecting surface 3" in length, high-alumina ceramic tube insulator with 3/8" inner diameter and ½" outer diameter and 3.5" in length, and a stainless steel outer conducting ring of approximately the same inner diameter of the insulator with a outer diameter of 5/8"and 3" in length.

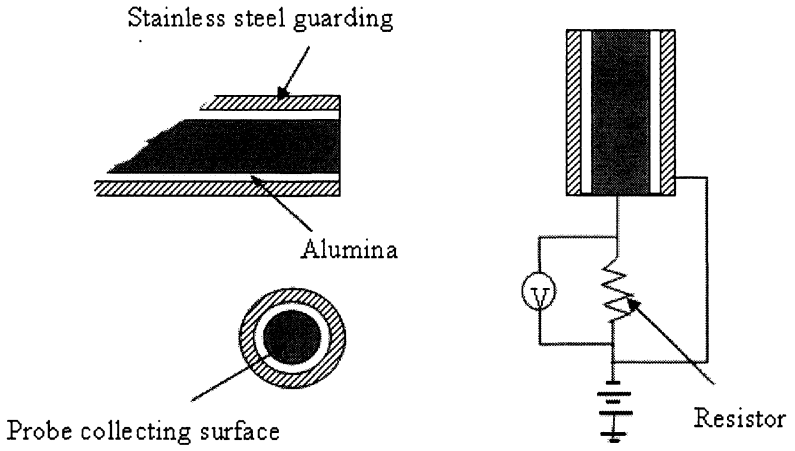

Figure 3.4 Faraday probe configuration (Schuettpelz, et al. 9-12 July 2006)

The probe collecting surface wiring was connected at the back of the probe and fed through a connecting stainless tube. The connecting tube with was negatively biased with respect to the ground and connected to the outer conducting ring, therefore biasing it. This was done by connecting a wire to the bottom of the connecting tube that fed through the vacuum wall with a BNC feedthrough. The probe collecting surface wiring is insulated from the ground and outer collecting surface. Faraday probes are widely used in plasma studies because they provide decent accuracy and are very inexpensive to build.

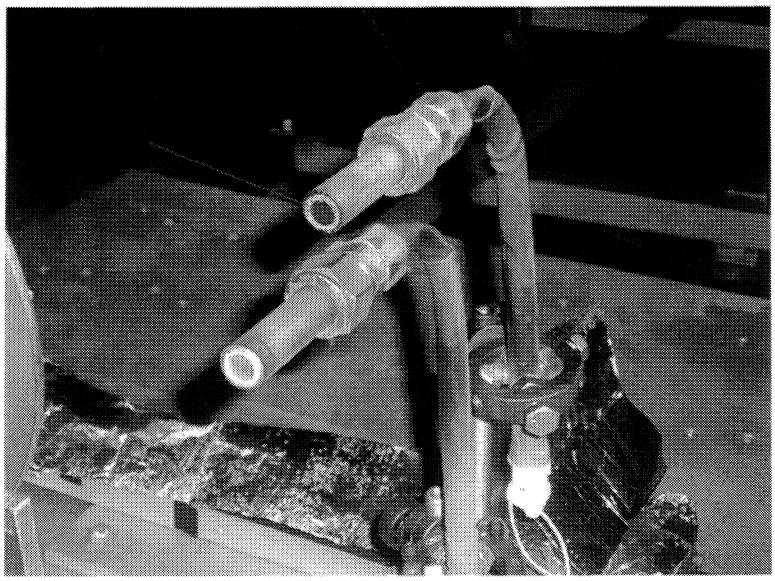

Figure 3.5 Faraday probes

The probes were swept from left to right across the plume on a Velmex 2-D stepper motor actuator driven by a Warner Electric and Superior stepper motors. The actuator was controller manually with a Velmex VP9000 controller. The PPS was

covered with aluminum foil to protect it from ionic impact that could cause erosion, shown in Figure 3.6.

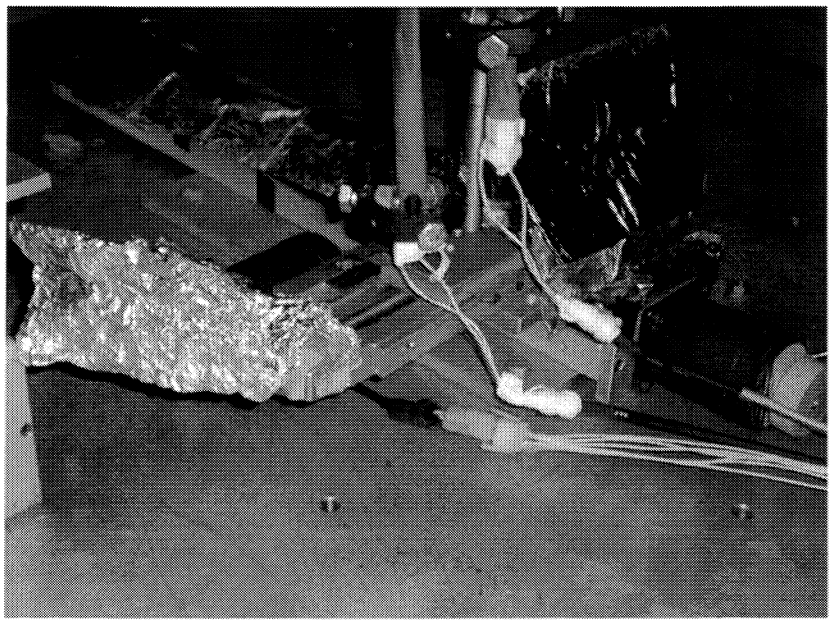

Figure 3.6 PPS

Current collected from the two probes is fed through wiring connected at the rear end of the collecting surfaces, then to a Hewlett Packard 500 MHz/ 1GSa/s Infinium oscilloscope. Two BNC vacuum wall feedthroughs connected the wiring from probes inside of the chamber to the oscilloscope wiring on the outside of the chamber. The resistance in both of the probe circuits is 50 ohms.

The Faraday probe sweeps are used to determine beam divergence by using the plume density profiles, and the divergence was measured for various beam voltages. The operating parameters displayed on the PPU front panel are used to calculate thrust, specific impulse, and efficiency (not including the beam divergence losses). Those results are then used as inputs to CHEBYTOP to perform the Mars and Jupiter mission analyses.

The procedures for interpreting and analyzing that data will be discussed in the following chapter.

CHAPTER 4

DATA ANALYSIS & MODELING

The primary purpose of this work was to study the effects of beam voltage on trip time and propellant fraction for missions of interest. We chose to use CHEBYTOP for the mission analysis. CHEBYTOP is a general purpose two-body, sun-centered, low thrust trajectory optimization and analysis tool which is typically used for preliminary mission studies. This code was chosen since it has a fast run time and is not difficult to learn. In general the procedure to acquire and analyze these inputs is as follows: Once the thruster is operational at desired beam voltage, PPU parameters are recorded from the PPU display. The probes are then swept from left to right across the plume on the probe positioning system. Data captured by the DAQ system is saved as x-y time steps and is analyzed in MathCAD and Excel to find divergence. Similarly, the readings from the display of the PPU and diversion results are used to find the inputs for the mission analysis. Below we provide a discussion of the motivation for the study, the data acquisition procedures, analysis of the data and a brief description of CHEBYTOP.

4.1. Motivation

Ion thruster inefficiencies result in reduced performance, which results in lower thrust, lower specific impulse, heavier PPU mass, longer trip times, smaller payloads, and increased launch cost. Most of the causes for ion thruster inefficiencies are well

understood, and some devices have reportedly reached efficiencies of 80% (Sutton and Biblarz 2001). One of the sources is the beam divergence angle, as discussed in Chapter 2. According to the manual (Group July 2004), while the beam voltage controls the thrust and specific impulse, it has an undetermined yet measurable effect on the beam divergence angle. Originally, we tried to determine a relationship between beam voltage and the divergence angle. However, our results were consistent with statements in the manual, and realized that the relationship was nebulous. We recognized that in order to grasp the effects, we would have to estimate some upper and lower bounds on the efficiency. Therefore, we decided to perform some mission studies using these upper and lower bounds on beam divergence efficiency to qualify the effect. To our knowledge, such a study has not been performed before and been formalized.

4.2. Data Acquisition System

The DAQ was used to record beam currents during Faraday probe sweeps across the ion thruster plume. The beam current profile produced from these data allows us to determine the beam divergence angle. One of the main challenges in the procedure was related to the finite memory buffer length on the DAQ system and the lack of an automated timing mechanism for turning on the system while performing a probe scan. We used an approximate relation, which allowed an appropriate synchronization between the delay time on the probe sweep and the acquisition time, given by

$$T_A \approx \frac{B}{S} \approx T_D, \tag{4.1}$$

where T_A is the acquisition time, B is the buffer size, S is the sample rate, and T_D is the delay time. The max buffer size of the DAQ system was 32,000 samples, and setting the

sample rate at 500 samples per second produced acquisition and delay times of approximately one minute.

To calibrate the DAQ system a B&K Precision 3020 Sweep/Function Generator was used. After observing the T_A as a result of timed test sweeps, the function generator was connected to the DAQ system through BNC cables and multiple functions were generated. To find the T_D, which at first was not known to exist, different signals from the function generator were sent to the DAQ system for certain time periods. For example, a sine wave would be sent for ten seconds followed by a sawtooth function for another ten seconds and repeat. Knowing the duration of the signals and when they changed, the acquisition time and delay time could be found.

4.3. Data Acquisition and Test Matrix

A 2D parameter space was chosen for measuring beam divergence angle with beam voltage and axial probe position being the independent variables. The latter is necessary for determining the angle. We used the following procedure to perform the measurements in this space. A probe sweep is done at the lowest beam voltage at the shortest axial distance from the ion source, and this is repeated from lowest to highest voltage at fixed axial probe position. The probes are then moved to the next distance and sweeps are performed from lowest to highest voltage. This procedure is done for each distance and for each voltage.

The data acquired, time and voltage information, is transferred from the DAQ system to Excel to be formatted, and later to MathCAD to be analyzed. Similarly PPU output is recorded for each test and analyzed in MathCAD, where beam voltage was the only variable. A sweep is performed for beam voltages of 600 V, 800 V, 1000 V, 1200 V,

and 1400 V at 1", 1.5", 2", 2.5", and 3" from the source as shown in the test matrix in Table 4.1. Those beam voltages were chosen because they were close to NSTAR operating parameters (Hamley, et al. 1998) and those axial distances were chosen because they did not exceed the capabilities of the PPS. The distance represents the closest probe to the source; probe two is 2 and 3/8" from probe one.

Table 4.1 Test matrix

Axial Position (in)	Beam Voltage (V)	Beam Voltage (V)	Beam Voltage (V)	Beam Voltage (V)	Beam Voltage (V)
1.0	600	800	1000	1200	1400
1.5	600	800	1000	1200	1400
2.0	600	800	1000	1200	1400
2.5	600	800	1000	1200	1400
3.0	600	800	1000	1200	1400

4.4. Uncertainty Analysis

Overall uncertainty in the probe measurement is combination of the systematic uncertainty, S_{B_i}, and the random uncertainty, S_i, (Coleman and Steele Jr. 1999). S_{B_i} is found from the following relation,

$$S_{B_i} = \frac{B_i}{2}, \tag{4.2}$$

where B_i is the systematic uncertainty, which is assumed to be 5 % of measured voltage (Haas, et al. 1998). The random uncertainty is found from the following relation,

$$S_i = \frac{S_x}{\bar{X}}, \tag{4.3}$$

where S_X is standard deviation of the sample of N readings, and mean of the sample population found from the following equation,

$$\bar{X} = \frac{1}{N}\sum_{i=1}^{N} X_i, \tag{4.4}$$

where X_i is the individual readings.

To find S_i of the probe, a test was run with a stationary probe in the center of the plume approximately 20 seconds of T_A at a sample rate of 1000 samples per second. The data were placed in Excel where S_X and $\bar{X}$ were found and S_i was calculated with Equation (4.3). This resulted in a S_i of approximately 3% of the measured voltage. The combined standard uncertainty is then

$$u_c^2 = S_{B_i}^2 + S_i. \tag{4.5}$$

A level of confidence must be associated with uncertainty, and this found using the relation,

$$U_{\%} = t_{\%} u_c, \tag{4.6}$$

where $U_{\%}$ is the overall uncertainty and $t_{\%}$ is coverage factor. When N is greater than 10 $t_{\%}$ at a 95 % confidence level is approximately 2 ($t_{95} = 2$). Therefore the uncertainty band around the voltage measurement is $\pm U_{\%}$. The resulting uncertainty band for probe voltage measurements was approximately ± 7 % of the measured voltage.

To find the uncertainty of the divergence angle, an uncertainty propagation analysis must be done on probe measurements, as it is used to calculate beam divergence.

Beam divergence, θ, is the essentially the half of angle of ion thruster's plume, which can be calculated from the slope equation,

$$\theta = \tan^{-1}\left(\frac{y_{n+1} - y_n}{x_{n+1} - x_n}\right), \tag{4.7}$$

where x_n divergence at the initial distance from the source, y_n, and x_{n+1} is divergence at the next distance from the source, y_{n+1}. The uncertainty of divergence angle is then found from,

$$U_\theta^2 = \left(\frac{\partial\theta}{\partial y_{n+1}}\right)^2 U_{y_{n+1}}^2 + \left(\frac{\partial\theta}{\partial y_n}\right)^2 U_{y_n}^2 + \left(\frac{\partial\theta}{\partial x_{n+1}}\right)^2 U_{x_{n+1}}^2 + \left(\frac{\partial\theta}{\partial x_n}\right)^2 U_{x_n}^2, \tag{4.8}$$

where $U_{y_{n+1}}$ and U_{y_n} are the overall uncertainties of the y_{n+1} and y_n positions respectively, and $U_{x_{n+1}}$ and U_{x_n} are the overall uncertainties of the x_{n+1} and x_n divergences. The distances from the source can be measured very accurately; therefore, $U_{y_{n+1}}$ and U_{y_n} are assumed negligible. Taking the partials of the above equation and neglecting $U_{y_{n+1}}$ and U_{y_n}, U_θ becomes

$$U_\theta^2 = \left[\frac{\dfrac{(y_{n+1} - y_n)^2(-1)}{(x_{n+1} - x_n)^2}}{1 + \left(\dfrac{(y_{n+1} - y_n)}{(x_{n+1} - x_n)}\right)^2}\right]^2 U_{x_{n+1}}^2 + \left[\frac{\dfrac{(y_{n+1} - y_n)^2}{(x_{n+1} - x_n)^2}}{1 + \left(\dfrac{(y_{n+1} - y_n)}{(x_{n+1} - x_n)}\right)^2}\right]^2 U_{x_n}^2. \tag{4.9}$$

The uncertainty of the divergence angle is calculated at each slope interval, which is from distances of 1'' to 2'', 2'' to 3'', 3'' to 4'', and 4'' to 5'' from the source. Since they were measured with the same probe, $U_{x_{n+1}}$ and U_{x_n} are taken to be 7 %. The results of the slope intervals were averaged to find U_θ of the edge. This was repeated for the

other edge, and the overall U_θ is the average of the left edge and right edge U_θ's as shown below,

$$U_{\theta overall} = \frac{U_{\theta left-avg} + U_{\theta right-avg}}{2}, \tag{4.10}$$

where $U_{\theta left-avg}$ is the left edge average overall uncertainty of the divergence angle, and $U_{\theta right-avg}$ is similarly for the right edge. This procedure was done for both probes for all the tests.

4.5. Beam Divergence Analysis

The plume sweep produces an ion current density profile. Assuming that 10 % of the peak voltage represents the left and right edges of the plume and the peak represents the centerline of the plume, the beam divergence can be found. This is calculated using the measured width plume at fixed voltage at each axial location. The axial coordinates of the probe are actually determined by knowing the probe sweep velocity and a reference position at some known time for the probe. The positioning system has a translational velocity (v_t) of 0.3125inch/sec and the DAQ acquisition rate of 500 sample/sec. The divergence from plume centerline is found from the following relations:

$$Left\ divergence\ (inch) =$$

$$\left(x_{peak} - x_{10\%left}\right)\frac{0.3125\left(inch/\sec\right)}{500\left(sample/\sec\right)}, \tag{4.11}$$

$$Right\ divergence\ (inch) =$$

$$\left(x_{peak} - x_{10\%right}\right)\frac{0.3125\left(inch/\sec\right)}{500\left(sample/\sec\right)}, \tag{4.12}$$

where x is the sweep positions.

Divergence calculations are plotted with respect to distance from the source, and a linear regression is done on both the left and right edges to find the slope of the lines. The angle in radians of the lines is found with the following relation:

$$\theta_{radians} = \tan^{-1}(slope). \tag{4.13}$$

The angle in degrees in found from

$$\theta_{degrees} = \theta_{radians}\left(\frac{\pi}{180}\right). \tag{4.14}$$

4.6. Thrust & Efficiency Analysis

Performance parameters such as thrust, specific impulse, divergence efficiency, and overall efficiency are important ion thruster performance parameters. These parameters play an important role in determining the feasibility of mission. Therefore, in this research, parameters are determined using experimental results. Some of these results are subsequently applied in Mars and Jupiter mission analyses to determine mission performance. The procedures for determining these parameters are discussed in the following sections.

4.6.1. Thrust Analysis

During thruster operation, the readings on PPU front panel display are the thruster operational parameters, shown in Figure 4.1. The most important one for this research, the beam voltage, is changed for each test, whereas, the other parameters are mostly kept constant. The PPU display parameters kept mostly constant are filament current (I_F)

and voltage (V_F), discharge current (I_D) and voltage (V_D), accelerator current (I_A) and voltage (V_A), and beam current (I_B). The term "mostly" is used because parameters such as the discharge current and beam current are measurements, and vary by a very small percentage throughout testing and sometimes not at all; therefore, it can be safe to assume they are constant. Also, the front panel argon gas flow $(\dot{m}_{Ar})$ and voltage bias are kept constant throughout the tests. Using these constant parameters, at varying beam voltages, thrust, specific impulse, and efficiencies can be found using the methods described below.

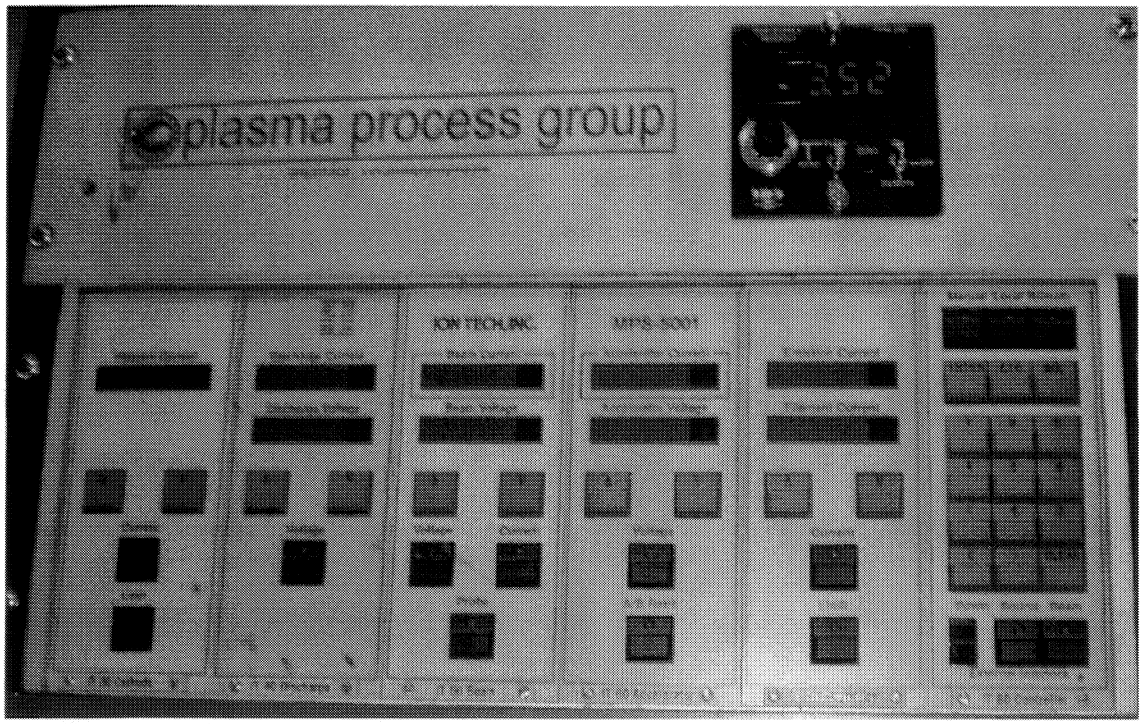

Figure 4.1 PPU front panel

The exhaust velocity of ions leaving the thruster are found using this relation found in Jahn (1996):

$$v_e = \left(\frac{2qV_0}{M} \right)^{1/2}, \tag{4.15}$$

where $V_0 = V_B - V_A$, q is the electric charge (1.6002 x 10^{-19} Coulombs), and M is the molecular weight of Argon. From this, the specific impulse is found with

$$I_{sp} = \frac{v_e}{g_0}, \tag{4.16}$$

where g_0 is 9.807 m/s^2. The thrust can now be found from Jahn (1996) using the relation:

$$T_{ion} = \left(\frac{\pi}{4} \right) D^2 \cdot \left(8 \frac{\varepsilon_0}{9} \right) \cdot \left(\frac{V_0}{x_a} \right)^2, \tag{4.17}$$

where D is the source diameter (8 cm), ε_0 is the permittivity of free space, and x_a is the distance between the accelerator grids.

4.6.2. Efficiency Analysis

The overall efficiency of an ion thruster is mainly a function of the PPU system efficiency and efficiency of the thruster itself. These two efficiencies essentially show how effectively 'wall plug' power is converted into jet power. Sources of inefficiency can be accounted for in terms of the power dissipated in each mechanism, and for completeness we discuss estimates for these here.

The process of ionization requires power since energy must be transferred to the propellant to liberate an outer electron from the shell of the atomic species. This is some factor times the ionization potential that is highly dependent on the ionization process and propellant. A reasonable estimate for electron bombardment ionization is given as

$$P_{ion} = 300\left(1.6\times10^{-19}\,Joules\right)\frac{\dot{m}_{Ar}}{M}, \tag{4.18}$$

where the 300 is the ionization cost of argon in eV/ion. The beam power is given by

$$P_B = \frac{1}{2}\dot{m}_{Ar}v_e^2, \tag{4.19}$$

and represents the useful jet power of the exhaust, and is needed to calculate the mass utilization efficiency.

Mass utilization efficiency refers to the fact that some finite amount of neutral atoms will leave the system without undergoing significant acceleration, and therefore hurt the overall specific impulse. The ion mass flow rate is,

$$\dot{m}_{ion} = \frac{I_B \cdot M}{q}. \tag{4.20}$$

In terms of this flow rate, the mass utilization efficiency is,

$$\eta_{util} = \frac{\dot{m}_{ion}}{\dot{m}_{gas}}, \tag{4.21}$$

and the power consumed by utilization is,

$$P_{util} = P_B\left(1-\eta_{util}\right). \tag{4.22}$$

The thruster power was then found from this equation:

$$P_{thruser} = P_B + P_{ion} + P_{util}. \tag{4.23}$$

Total power of the system is the summation of accelerator grid power, P_A, discharge power, P_D, filament power, P_F, and beam power:

$$P_{total} = P_A + P_D + P_F + P_B. \tag{4.24}$$

Once the powers are calculated, the efficiencies can be found from the following relations:

$$\eta_{PPU} = \frac{P_B}{P_{total}}, \tag{4.25}$$

$$\eta_{thruster} = \frac{P_B}{P_{thruster}}, \tag{4.26}$$

and

$$\eta_{overall} = \eta_{ppu} \cdot \eta_{thruster}, \tag{4.27}$$

where those are the PPU system efficiency, thruster efficiency, and overall efficiency, respectively. To take plume diversion into consideration, the diversion efficiency has to found from the following relation:

$$\eta_D = \frac{1}{\theta}\int_0^{\theta} \cos\theta' d\theta'. \tag{4.28}$$

Taking the integral, this equation becomes

$$\eta_D = \frac{1}{\theta}\sin\theta'\Big|_0^{\theta}. \tag{4.29}$$

The diversion efficiency is then,

$$\eta_D = \frac{1}{\theta}\sin\theta. \tag{4.30}$$

The overall system efficiency is then,

$$\eta_{overall} = \eta_{ppu} \cdot \eta_{thruster} \cdot \eta_D. \tag{4.31}$$

4.7. Mission Analysis

We chose to use CHEBYTOP for the mission analysis, which is a general purpose two-body, sun-centered, low thrust trajectory optimization and analysis tool. This model is typically utilized for preliminary mission studies. It was an attractive approach for the

current study since it has a small number of inputs and produces very quickly, and is regarded as a valuable tool by those in the field who perform mission feasibility studies.

CHEBYTOP takes a user defined desired trip time along with other inputs and optimizes a mission using the two-body equations of motion for an interplanetary vehicle,

$$\ddot{x} + \frac{kx}{r^3} = a \quad 0 \le t \le T, \tag{4.32}$$

where $x(t)$ is the position vector of the vehicle, $a = a(t)$ is applied acceleration vector, k is the gravitational constant of the sun, $r = |x|$, and T is the trip time. Using the above equation, the program optimizes thrust and acceleration using the defined inputs, and using orbital mechanics finds the best trajectory and trip time. With these parameters known, other mission parameters can be determined.

Using thruster performance determined with the above procedure, we used specific impulse and efficiency as inputs into CHEBYTOP to perform some mission studies for LEO to Mars and LEO to Jupiter. We made assumptions for the other inputs required using information from the literature, including specific mass, PPU system mass, overall efficiency, tankage fraction, initial mass, initial power, LEO orbit, arrival planet parking orbits and radii, and an assumed mission duration.

The PPU system mass was found from this relation:

$$PPU\ sytem\ mass = P_{total} \times I_{sp}. \tag{4.33}$$

The initial mass was found by combining all the component masses including solar array mass, thruster mass, DCIU mass, and the gas feed sytem mass. The DCIU and gas feed system masses were from the NSTAR (Polk, et al. 2000), and the thruster mass is a

manufacturer's spec. The solar array mass was calculated using the specific power of the solar array used on the NSTAR engine (Murphy):

$$Solar\ Array\ Mass = P_{total} \div Specific\ power\ (solar\ array). \tag{4.34}$$

The initial power is the total power for that beam voltage, and the tankage fraction is from the NEXT Ion engine (Oleson, et al. 2002). Also, the total specific mass for each beam voltage, α, be found from the following relation:

$$\alpha = \frac{Power\ and\ Propulsion\ System\ Mass}{Total\ Power} = \frac{PPU\ Mass + Solar\ Array\ Mass + Thuster\ Mass + DCIU\ Mass}{Total\ Power}. \tag{4.35}$$

The arrival planet parking orbit is the desired orbital altitude of Mars or Jupiter for the orbit transfer from LEO. For Mars, that altitude is 60,000 km (Dailey, et al. 1991), for Jupiter it is 600,989 km (Polsgrove, et al. 2006), whereas the altitude of LEO is 550 km. The arrival planet parking radius is just the radius of the arrival planet plus the parking orbit. For Mars the parking orbit radius is 63,396 km and for Jupiter 672,481 km.

For the Mars and Jupiter missions, the inputs were put in at varying specific impulse, overall efficiency, PPU system mass, initial power, and initial weight for the lowest and highest η_D for each beam voltage. For the separate missions, the arrival planet parking orbit and radius, and mission duration was changed. For both missions specific mass, departure planet parking orbit and tankage fraction were held constant.

CHAPTER 5

RESULTS & DISCUSSION

Beam divergence measurements were taken using our 8 cm ion thruster. The 8-cm ion thruster was operated as closely as possible to the manufacturers specified operating conditions, Table 5.1. However, the gas flow had to be doubled from 5 sccm to 10 sccm to maintain an appropriate discharge current. If the gas flow is too low, the discharge current goes below the operation point for thruster, resulting in the thruster not creating plasma. Discharge current is a very important operational parameter because this current controls the ion production rate (July 2004). The only parameter intentionally each test changed was the beam voltage. Some parameters varied slightly with changes in beam power, but not by that much and thus are considered constants. The beam voltage was varied in accordance with Table 4.1. The neutralizer was turned off for more accurate ion profile measurements.

Table 5.1 Ion thruster operating conditions

Gas Flow (sccm)	Gas Type	Chamber Pressure (Torr)	Cathode Filament Heater (A)	Discharge Current (A)	Discharge Voltage (V)	Beam Current (mA)	Beam Voltage (V)	Accelerator Current (mA)	Accelerator Voltage (V)	Neutralizer Heater Current (A)	Neutralizer Emission Current (mA)
10	Argon	2.5×10^{-5}	4.63	0.37	55	91	600-1400	6	100	0	0

5.1. Uncertainty Results

The overall uncertainty results are shown below.

Table 5.2 U_θ (degrees) for Test 1

Beam Voltage (V)	600	800	1000	1200	1400
Probe 1	1.695549	1.885113	1.883354	1.73416	1.864497
Probe 2	1.975375	1.816863	1.878089	1.963415	1.903044

Table 5.3 U_θ (degrees) for Test 2

Beam Voltage (V)	600	800	1000	1200	1400
Probe 1	2.162315	2.131664	2.119055	2.117176	2.121375
Probe 2	1.928449	1.82709	1.998383	2.051149	1.974837

As seen above U_θ varies from about 1.696 to 2.162. Consequently, we assumed that for each beam divergence angle calculation there is an uncertainty of $2°$.

5.2. Beam Divergence Results

Two data sets were taken with same thruster operating conditions. For each data set, the divergence was found for both probes during each sweep at different beam voltages. The average divergence is found from the relation,

$$\theta_{avg} = \frac{\theta_{probe1} + \theta_{probe2}}{2}, \tag{5.1}$$

where θ_{probe1} and θ_{probe2} are the divergences from probe 1 and probe 2, respectively. This calculation was done for all beam voltages and both data sets. The results are given in Table 5.2 and plotted in Figure 5.1 with the 2° uncertainty bands.

Table 5.4 Average divergence results

	Data Set 1	Data Set 2
V_B (V)	θ (deg)	θ (deg)
600	31.4848	15.4696
800	19.5828	18.8617
1000	24.8531	18.3899
1200	23.6867	18.0859
1400	28.1456	17.7665

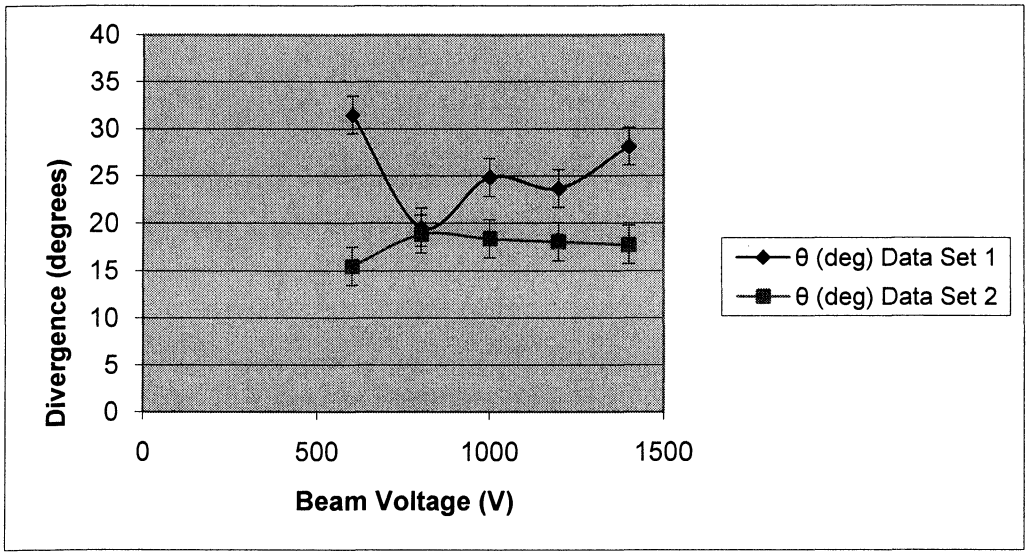

Figure 5.1 Average divergence vs beam voltage with uncertainty

These results show plume divergence as being somewhat random as beam voltage varies with highest and lowest divergence being at 600 V, which is consistent with observations made in the user's manual (July 2004). Consequently, we did not attempt to model the process. Rather, for the mission analysis, we interpret the results as providing an estimate on the beam divergence efficiency with a known uncertainty. To qualify this effect in terms of mission performance, we simply used the extremes of divergence efficiency and found the corresponding divergence angles to be 31.4848° and 15.4696°. This gives $\eta_{D-low\theta}$ and $\eta_{D-high\theta}$ of 99.7% and 98.7 %, respectively. We denote the overall efficiencies with $n_{overall-high\theta}$ and $n_{overall-low\theta}$.

5.3. Thrust & Efficiency Analysis Results

Table 5.3 summarizes our 8 cm ion thruster performance. Specific impulse increases the square root of beam voltage, shown in Figure 5.2, and thrust increases as the square of beam voltage, shown in Figure 5.3. These were calculated with equations 4.6-4.8. The overall efficiency varies with beam voltage mainly because of the increase in beam voltage. The beam voltage increase increases the accelerating potential, thus increasing exhaust velocity. With increases in specific impulse, available power and propellant is being more efficiently used, thus raising the overall efficiency (shown in Figure 5.4). The overall efficiency is only slightly better with a low divergence angle; nonetheless, this improvement in efficiency is due to a more focused exhaust plume, which creates a more axially directed thrust.

Table 5.5 Thrust & efficiency analysis results

V_B (V)	I_{sp} (s)	Thrust (mN)	$\eta_{overall\text{-}low\theta}$	$\eta_{overall\text{-}high\theta}$
600	5926	0.5385	0.332	0.328
800	6717	0.8901	0.364	0.361
1000	7426	1.33	0.387	0.384
1200	8073	1.857	0.405	0.401
1400	8672	2.473	0.418	0.414

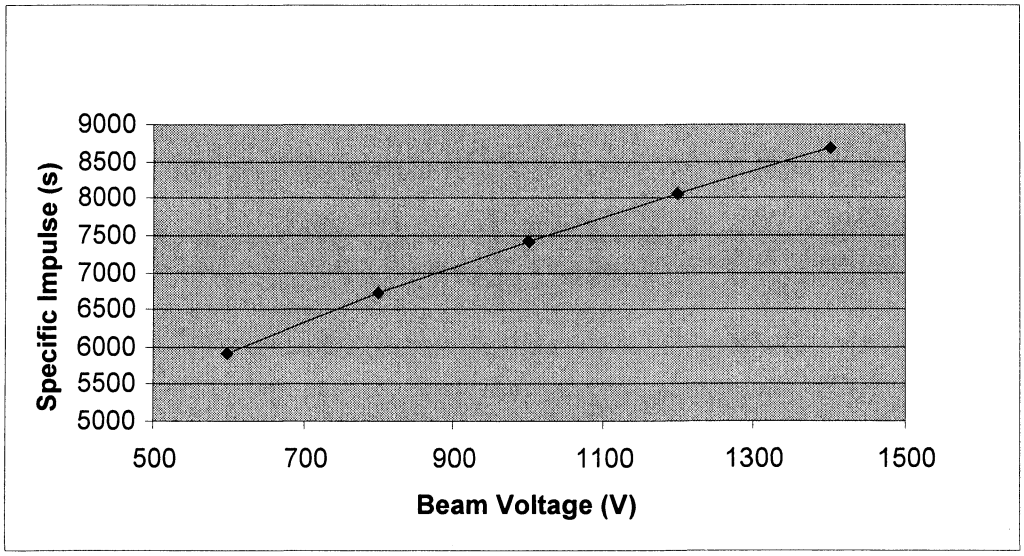

Figure 5.2 Specific impulse vs. beam voltage

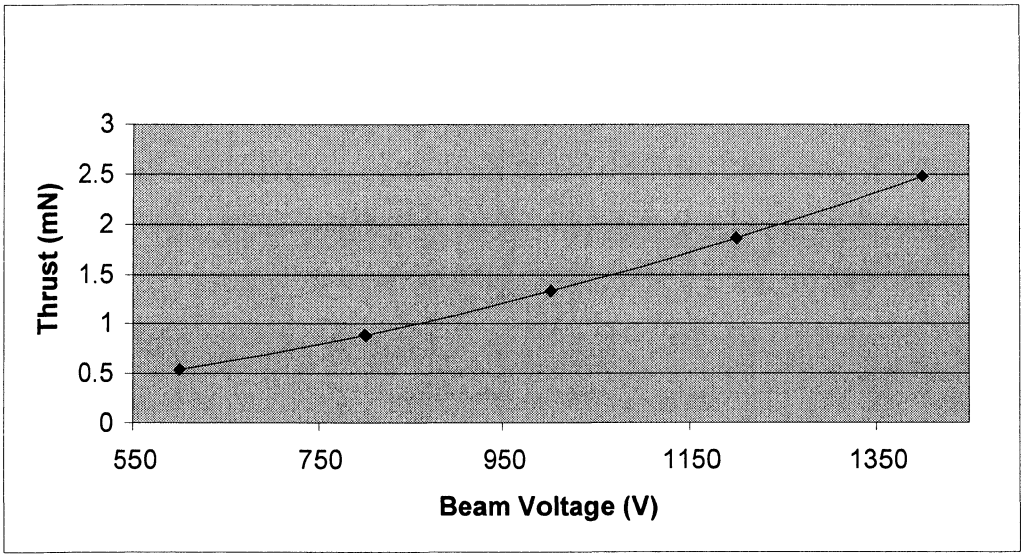

Figure 5.3 Thrust vs. beam voltage

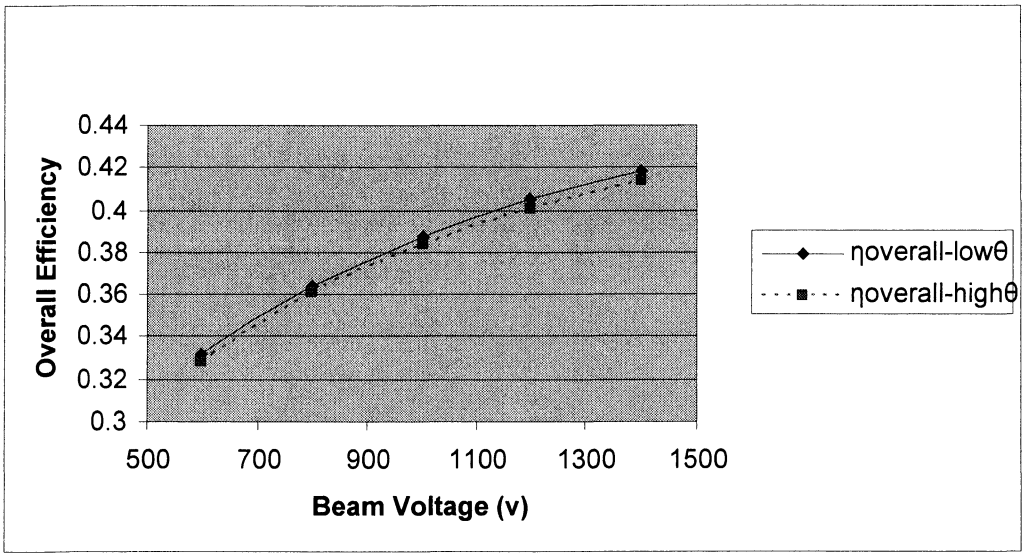

Figure 5.4 Overall efficiency vs. beam voltage

5.4. Chebytop Inputs

The inputs for the Mars and Jupiter missions varied with beam voltage and mission; some were constant, and a few came from thrust and efficiency analysis. These inputs are shown in the following tables.

Table 5.6 LEO to Mars/Jupiter mission inputs

V_B (V)	I_{sp} (s)	PPU Mass (kg)	Initial Mass (kg)	Initial Power (kW)	$\eta_{overall\text{-}low\theta}$	$\eta_{overall\text{-}high\theta}$
600	5926	4.42	51.12	.80373	0.332	0.328
800	6717	5.398	56.048	.981424	0.364	0.361
1000	7426	6.3745	60.9745	1.159	0.387	0.384
1200	8073	7.3535	65.8935	1.337	0.405	0.401
1400	8672	8.3325	70.8425	1.515	0.418	0.414

Table 5.7 Mission specific inputs

Mission	LEO to Mars	LEO to Jupiter
Parking orbit altitude (km)	60,000	600,989
Parking orbit radius (km)	63,396	672,481
Mission duration (days)	700	1200

Table 5.8 Input constants

Specific Mass (kg/kW)	LEO (km)	Tankage Fraction
30	550	0.025

The specific mass of 30 kg/kW was used as the total specific mass for each beam voltage and was at best in the thirties, so rounding down, this specific mass was used for all tests.

5.4.1. Chebytop Results

Tables 5.7 and 5.8 summarize the LEO to Mars mission analysis for the low and high beam divergence efficiencies, respectively. Trip time decreases as the beam voltage is increased, while the propellant fraction increases. The beam divergence has only a marginal effect on the mission results, which are plotted in Figure 5.5.

Table 5.9 LEO to Mars low divergence results

V_B (V)	Trip Time (Days)	Propellant fraction
600	1083.53	0.69252
800	1076.5	0.72348
1000	1070.93	0.74643
1200	1067.04	0.76428
1400	1064.03	0.77867

Table 5.10 LEO to Mars high divergence results

V_B (V)	Trip Time (Days)	Propellant fraction
600	1083.55	0.69251
800	1076.24	0.7234
1000	1071.02	0.74635
1200	1067.04	0.76428
1400	1063.97	0.77872

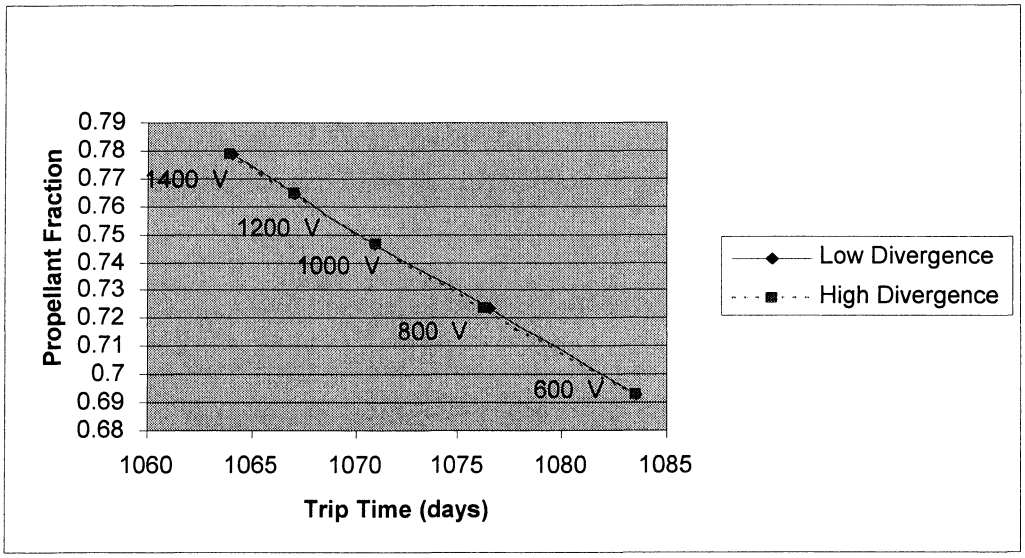

Figure 5.5 LEO to Mars propellant fraction vs. trip time

As expected, vehicle trip times from LEO to Jupiter are considerably longer, Tables 5.9 and 5.10. Qualitatively, the trends for the Jupiter mission are the same as those for Mars. Propellant fraction increases with beam voltage, while trip time decreases. The high divergence case gives only a negligible change in both trip time and propellant fraction at a fixed beam voltage, shown in Figure 5.6.

Table 5.11 LEO to Jupiter low divergence results

V_B (V)	Trip Time (Days)	Propellant fraction
600	1912.24	0.70501
800	1900.78	0.73245
1000	1889.15	0.75426
1200	1880.28	0.77134
1400	1823.55	0.7851

Table 5.12 LEO to Jupiter high divergence results

V_B (V)	Trip Time (Days)	Propellant fraction
600	1913.02	0.70472
800	1900.67	0.73249
1000	1888.98	0.75432
1200	1880.35	0.77132
1400	1823.53	0.7851

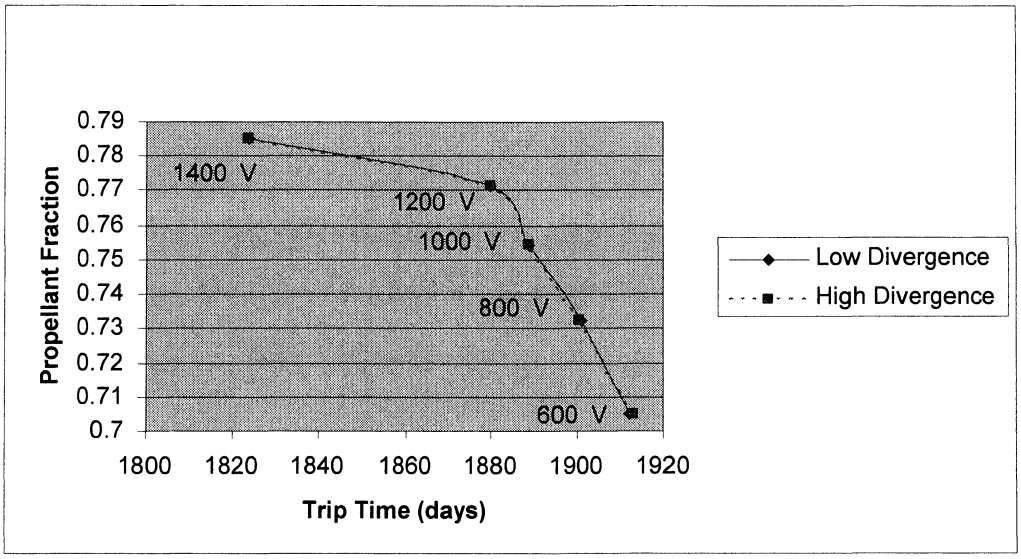

Figure 5.6 LEO to Jupiter propellant fraction vs trip time

These propellant fractions are relatively high, but this is because of the high v_e which results in a high I_{sp}. The v_e could theoretically be reduced by adding a decelerator grid on the ion thruster, which would go downstream of the screen grid. This is typically done for spaced-qualified thrusters in order to lower the specific impulse while not greatly sacrificing thrust, but such a grid is not part of our setup. To give an example of the decelerating grid effect, a case was run for both missions with an I_{sp} of 2000 s in CHEBYTOP. The case was run for high divergence at 1400 V for both Mars and Jupiter missions. The results are shown in Table 5.13, which shows reduced and more realistic propellant fractions.

Table 5.13 Low specific impulse results

Mission	Propellant fraction
Mars	0.36196
Jupiter	0.47213

The change in trends for beam voltage vs. vehicle trip time and propellant fraction as shown in Figure 5.5 for the Mars mission and Figure 5.6 for the Jupiter mission is due to the effects of the power supply penalty (Jahn 1996), in which there is an optimum specific impulse which can either minimize trip time or propellant fraction. For a constant thrust mission as was assumed in these Cheybytop runs, the propellant mass expelled Δm is related to the thrust $T_{mission}$, burn time t_b, and I_{sp} with,

$$\Delta m = t_b \frac{T_{mission}}{I_{sp} g_0}. \tag{5.2}$$

With these constraints, there is an optimum specific impulse (Jahn 1996) which minimizes waste mass (power supply plus propellant mass). Assuming a linear relationship between the required jet power and the power supply mass, the power supply mass is given by (Jahn 1996)

$$m_p = \frac{\alpha_m g_0 T_{mission} I_{sp}}{2\eta_{overall}}. \tag{5.3}$$

Summing these two masses and taking the derivative with respect to the specific impulse, we obtain

$$\hat{I}_{sp} = \frac{1}{g_0}\left(\frac{2\eta_{overall} t_b}{\alpha}\right)^{1/2}, \tag{5.4}$$

where $\hat{I}_{sp}$ is optimum mission specific impulse. It maximizes deliverable propellant fraction for a given mission (Jahn 1996).

CHAPTER 6

CONCLUSIONS

We studied the effects of beam voltage on divergence angle using experimental measurements from an 8 cm ion thruster. Specific mass, specific impulse, and efficiency were fed into CHEBYTOP, a low thrust in-space mission analysis tool, to determine trip time and propellant fraction for LEO to Mars and LEO to Jupiter. To the knowledge of the author, this is the first time that effects of beam divergence angle taken from experimental data have been used in such a study to quantify the impact on trip time and propellant fraction.

The beam voltage was varied between 600 and 1400 V. We scanned across the plume at various axial locations to measure the plume angle, in which the plume boundary was defined by 10 % of the peak beam current measured. Based on the analysis of the data, beam voltage, which controls the thrust density and specific impulse, has a strong, but undetermined effect on the beam divergence angle. In other words, the divergence angle varied with beam voltage, but the effect appeared to be random and not repeatable. The angle varied from 15 to 30 degrees with an uncertainty of 2°, which corresponds to a divergence angle efficiency between 99 and 95 %. Since beam voltage was found to have an almost random affect on the beam divergence angle, the highest and

lowest angles were taken as the worse and best case divergences for the thruster, and the mission analyses were performed for best and worst case scenarios. We found that the resulting divergence efficiencies were so high that their effect on overall efficiency, propellant fraction and trip times were negligible.

While the effects of beam voltage on vehicle performance are well known, the impact on various missions were of interest. Both trip times and propellant fraction were functions of the beam voltage. For both missions, higher beam voltages resulted in decreased trip time and an increase in propellant fraction, but the trip time only varied by about 5 % or less. This suggests that the optimum specific impulse, which minimizes travel time, is fairly close to our ion thruster operating conditions for missions between Mars and Jupiter.

The lowest beam voltage tested during this analysis was 600 V. We saw from the results that lower specific impulse values increase trip time for Mars missions. Future work with this thruster could do a test of beam voltages from 100-600 V. This could perhaps yield more efficient results for the Mars mission. As stated in the thruster manual, variations in accelerator grid more directly affect beam divergence. A beam divergence study combined with a mission study could be done varying the accelerator grid voltage with constant beam voltages to see if beam divergence has a more pronounced role on trip times and propellant fraction. Also, using a method called cross-correlation-velocimetry (Li, et al. 2004), the Faraday probes could be used to directly measure plume exhaust velocity using the plume frequency oscillations, to get an experimental measurement of specific impulse.

APPENDIX

BEAM DIVERGENCE PROFILES

The following figures show beam divergence profile with a linear curve fit for data sets 1 and 2. The individual data points are left (top) and right (bottom) plume edges at 1"to 3" from the ion source.

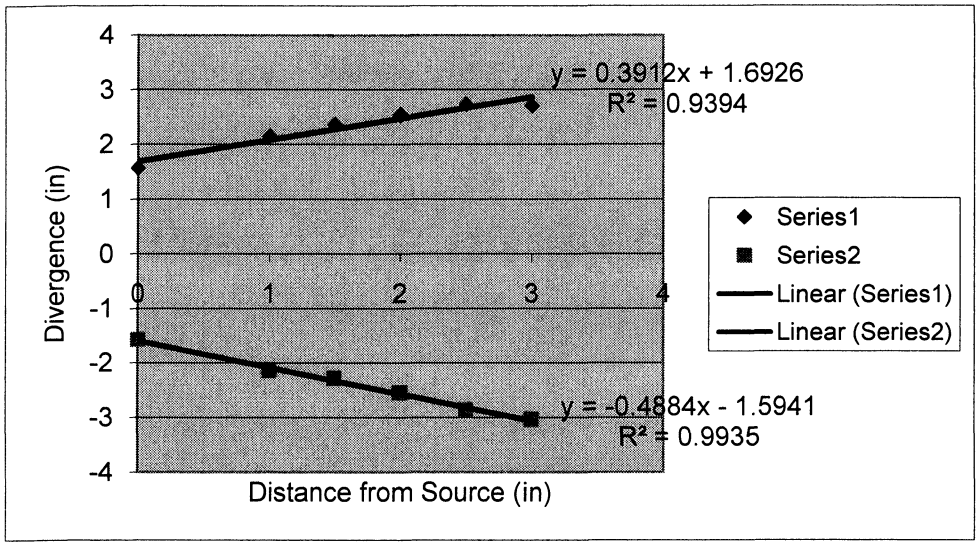

Figure A.1 600 V Beam Divergence Profile, Data Set 1, Probe 1

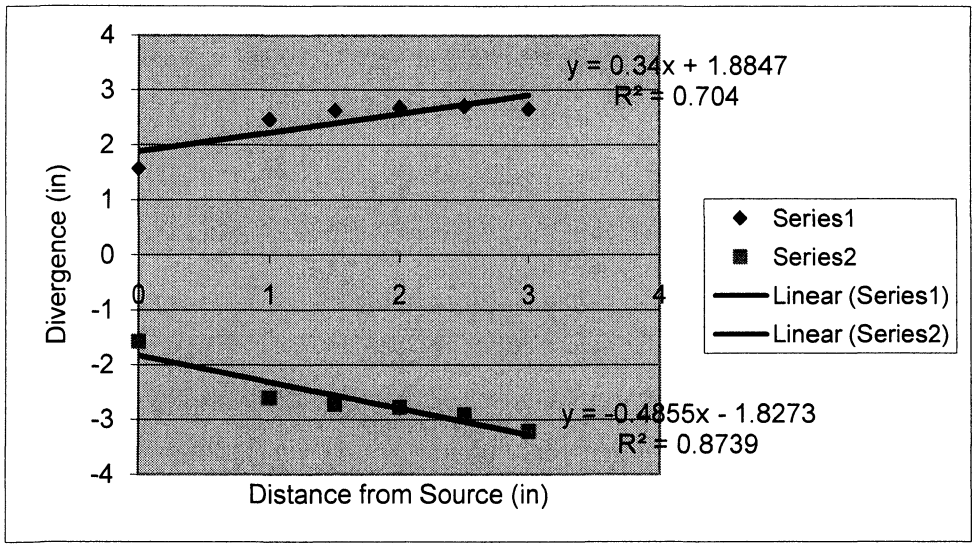

Figure A.2 600 V Beam Divergence Results, Data Set 1, Probe 2

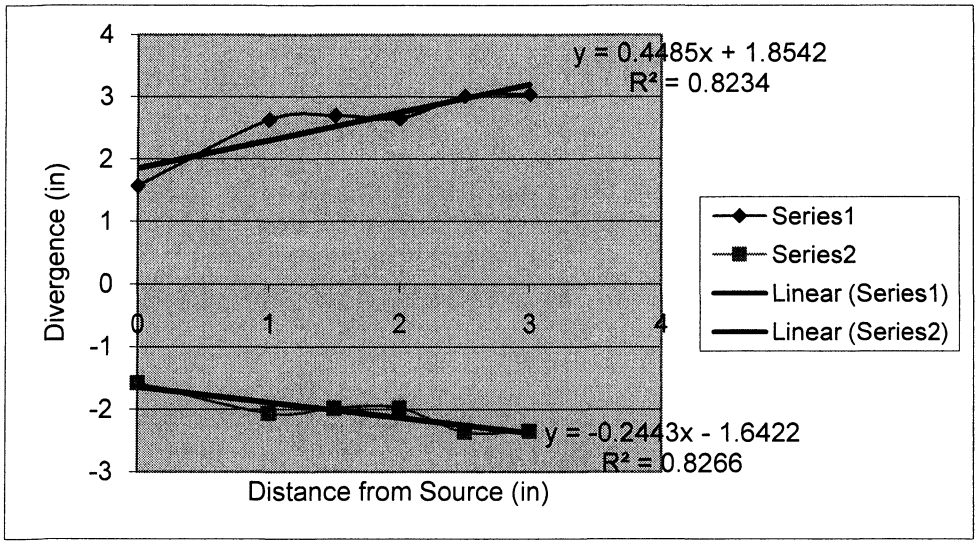

Figure A.3 800 V Beam Divergence Profile, Data Set 1, Probe 1

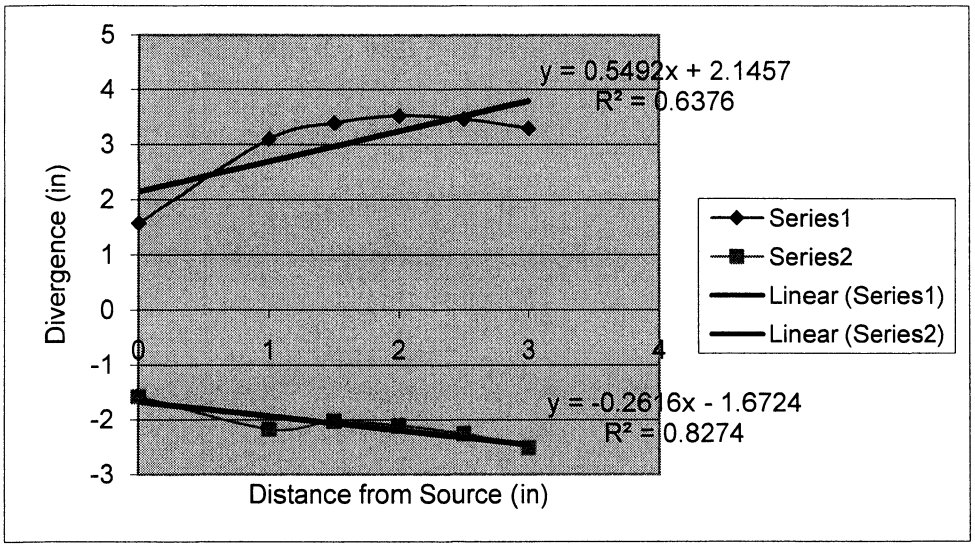

Figure A.4 800 V Beam Divergence Results, Data Set 1, Probe 2

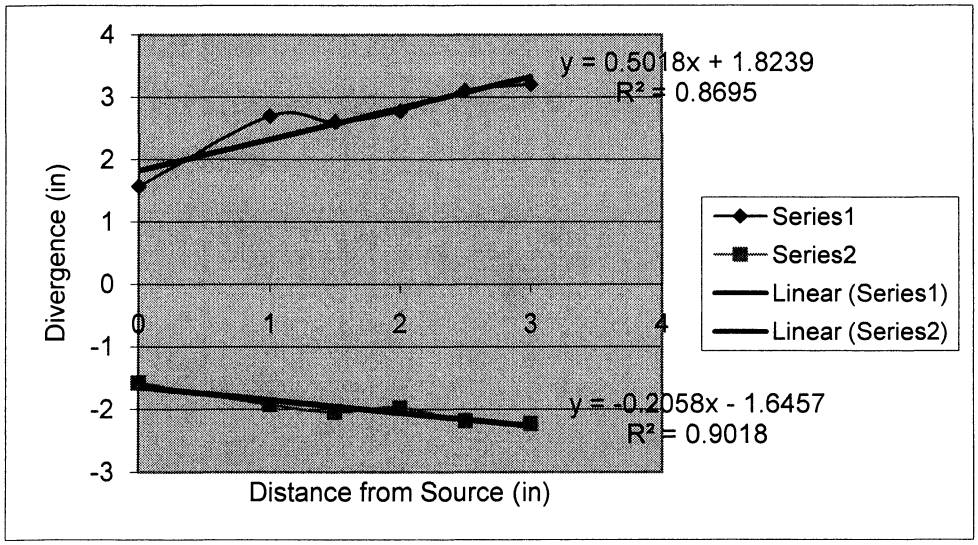

Figure A.5 1000 V Beam Divergence Profile, Data Set 1, Probe 1

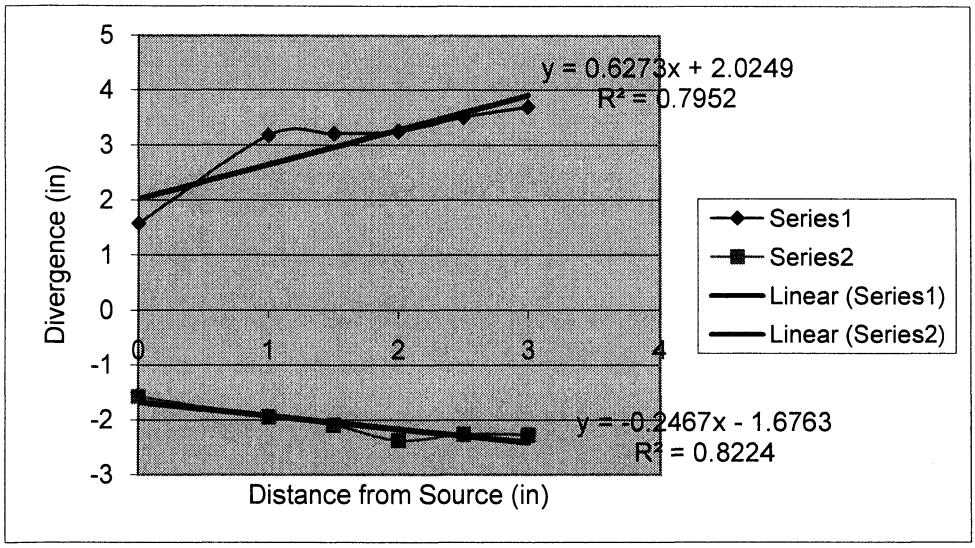

Figure A.6 1000 V Beam Divergence Results, Data Set 1, Probe 2

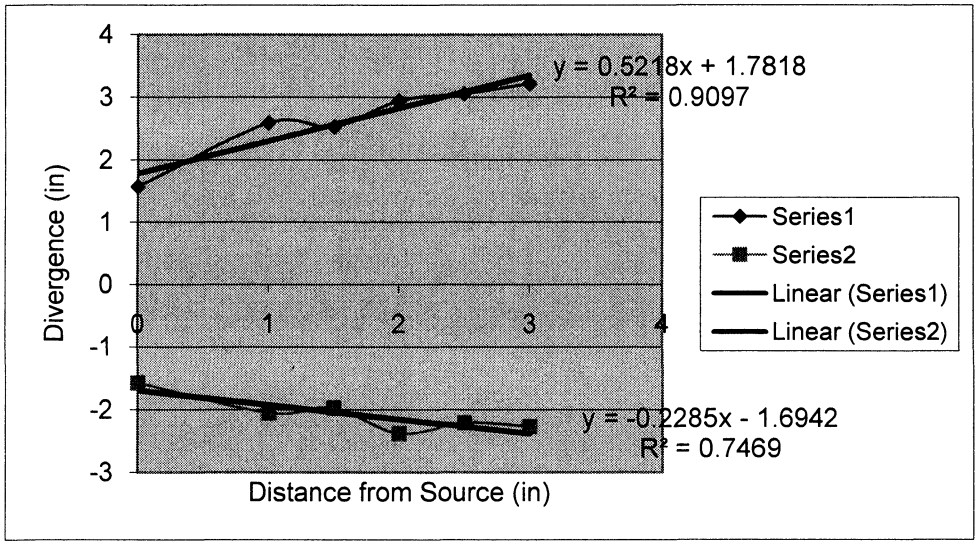

Figure A.7 1200 V Beam Divergence Profile, Data Set 1, Probe 1

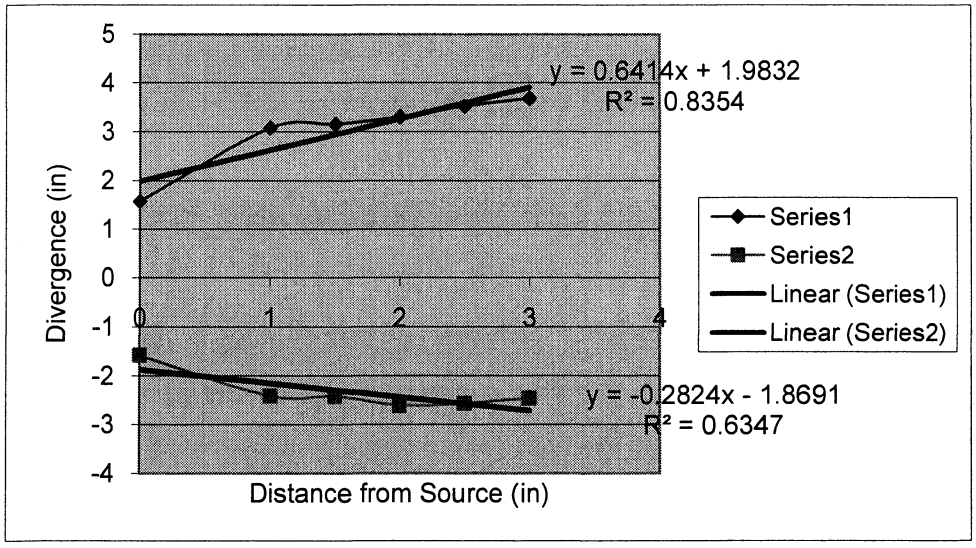

Figure A.8 1200 V Beam Divergence Results, Data Set 1, Probe 2

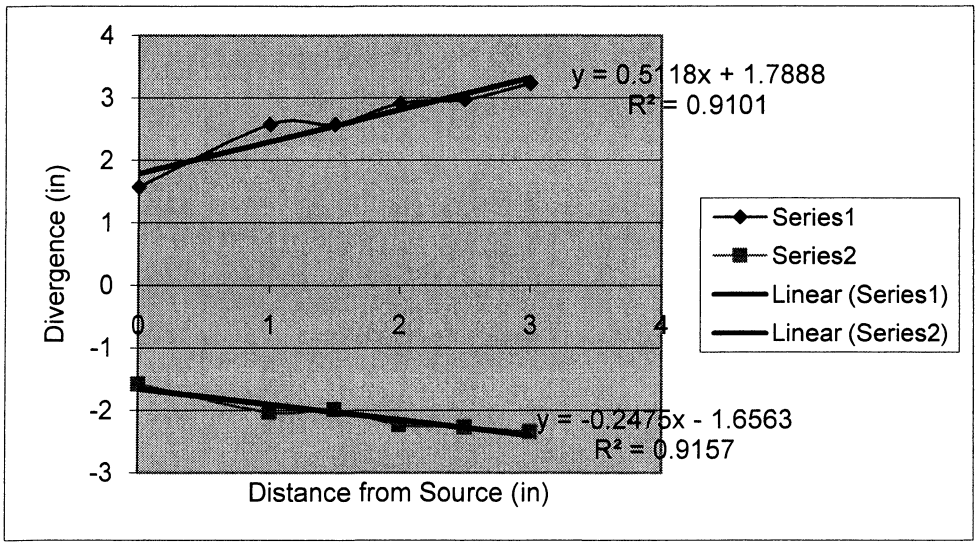

Figure A.9 1400 V Beam Divergence Profile, Data Set 1, Probe 1

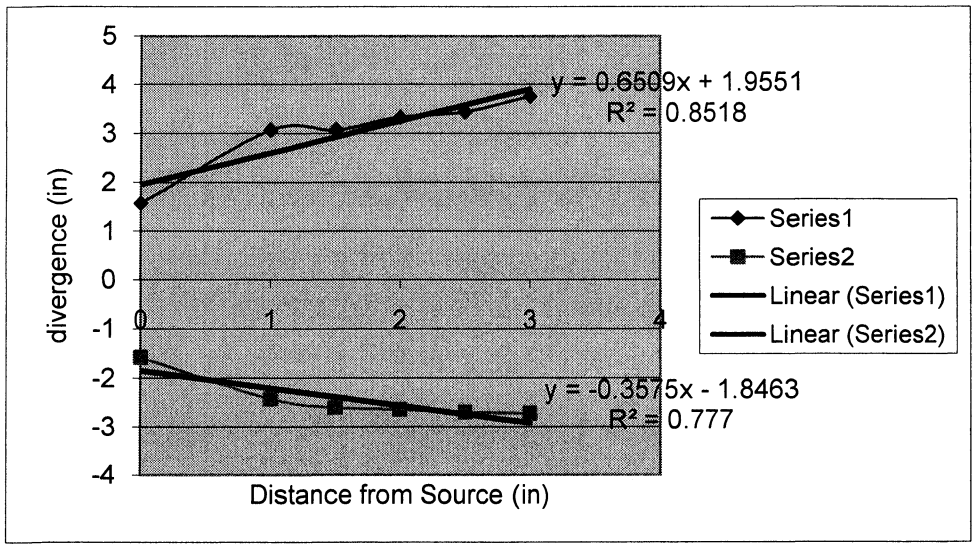

Figure A.10 1400 V Beam Divergence Results, Data Set 1, Probe 2

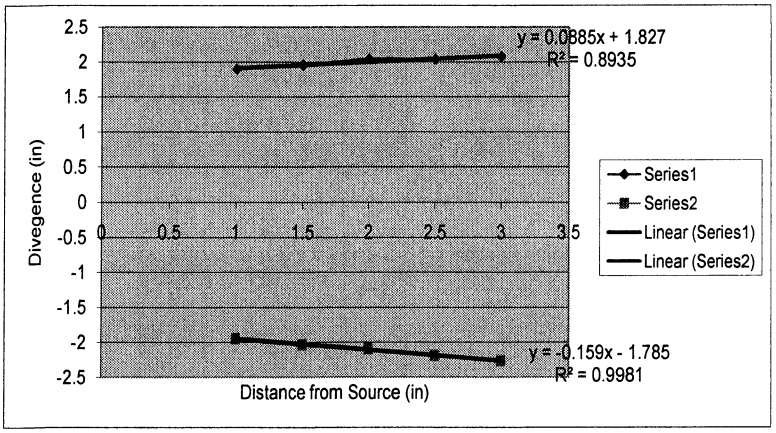

Figure A.11 600 V Beam Divergence Profile, Data Set 2, Probe 1

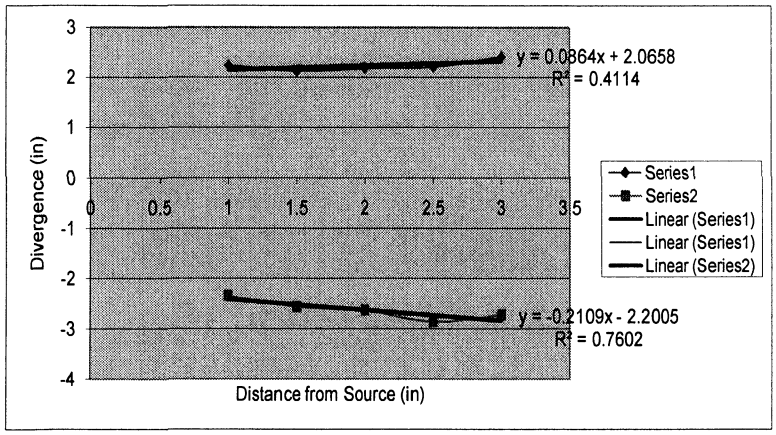

Figure A.12 600 V Beam Divergence Profile, Data Set 2, Probe 2

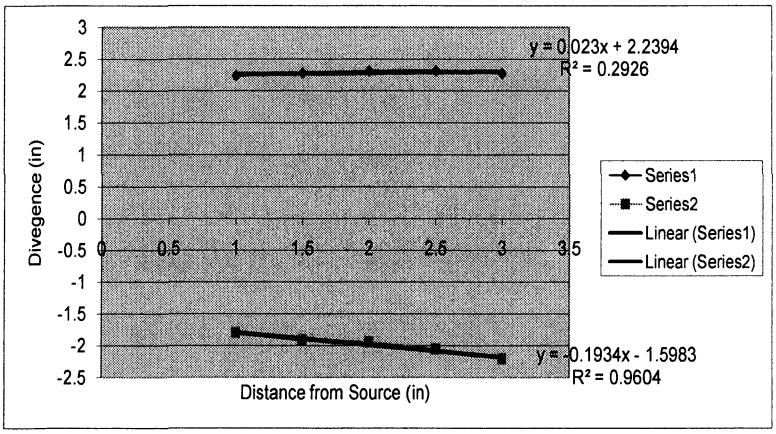

Figure A.13 800 V Beam Divergence Profile, Data Set 2, Probe 1

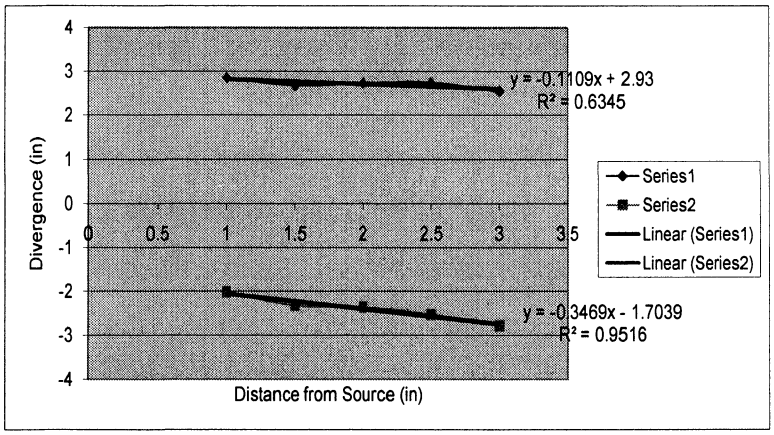

Figure A.14 800 V Beam Divergence Profile, Data Set 2, Probe 2

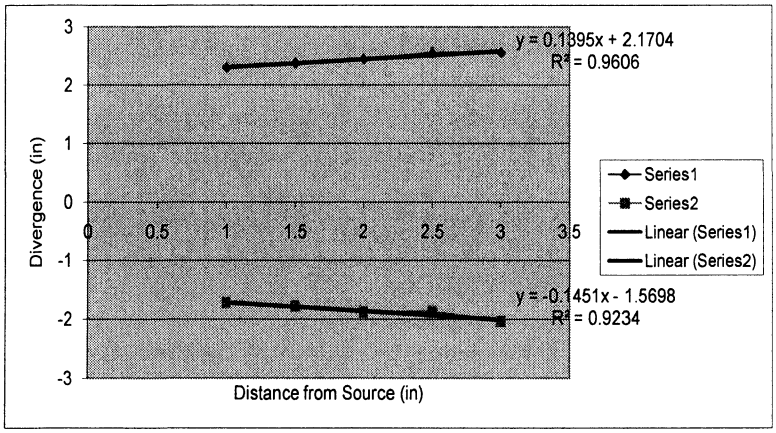

Figure A.15 1000 V Beam Divergence Profile, Data Set 2, Probe 1

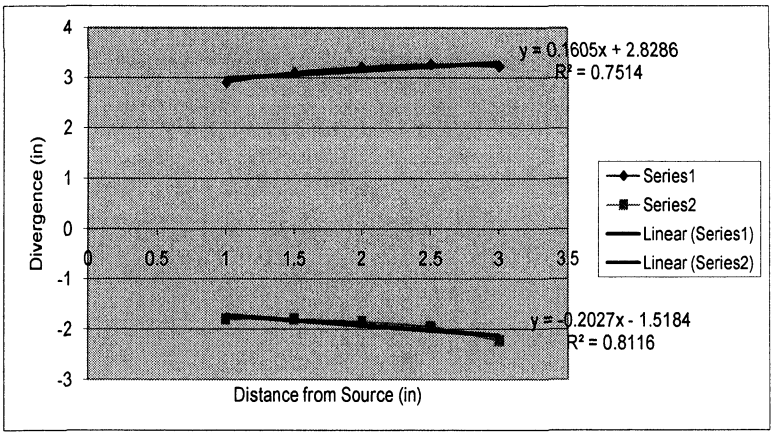

Figure A.16 1000 V Beam Divergence Profile, Data Set 2, Probe 2

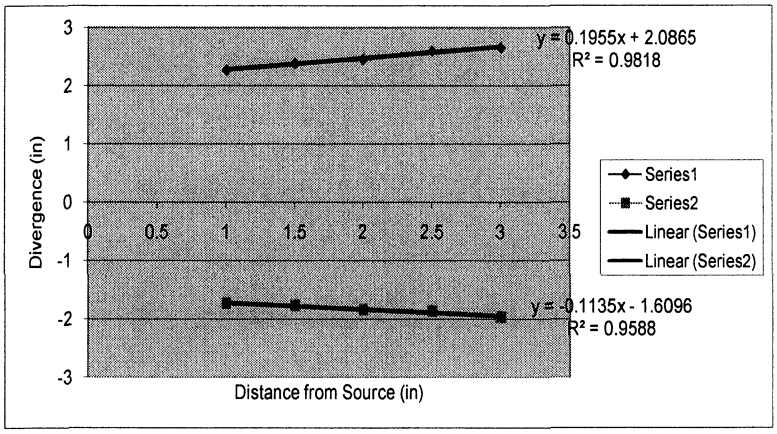

Figure A.17 1200 V Beam Divergence Profile, Data Set 2, Probe 1

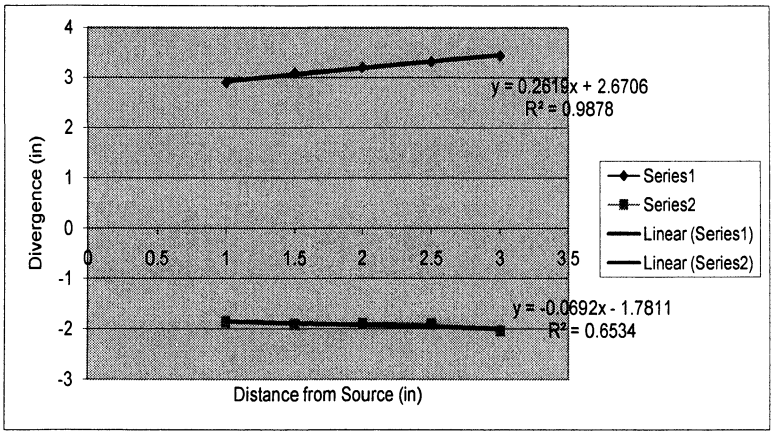

Figure A.18 1200 V Beam Divergence Profile, Data Set 2, Probe 2

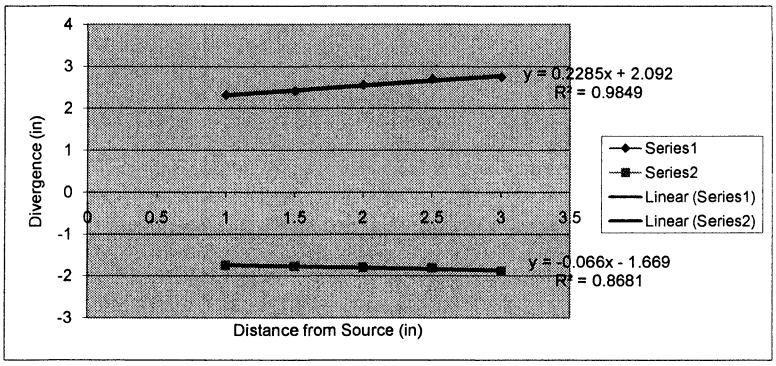

Figure A.19 1400 V Beam Divergence Profile, Data Set 2, Probe 1

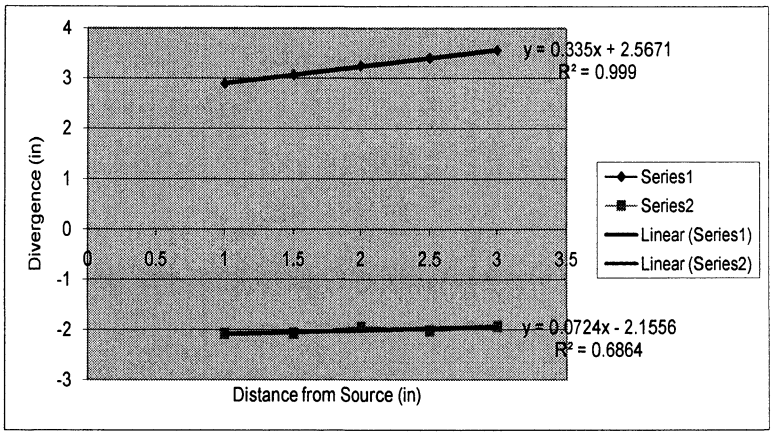

Figure A.20 1400 V Beam Divergence Profile, Data Set 2, Probe 2

REFERENCES

Beattie, J. R. (June 1998). "XIPS Keeps Satellites on Track." The Industrial Physicist.

Brophy, J. R. (2002). "NASA's Deep Space 1 Ion Engine." Review Scientific Instruments **73**: 1071-1078.

Brophy, J. R. (2002). "NASA Deep Space 1 Ion Engine (plenary)." Review of Scientific Instruments **73**(2).

Choueiri, E. Y. (2004). A Critical History of Electric Propulsion: The First Fifty Years (1906-1956). 40th AIAA/ASME/SAE/ASEE Joint Propusion Conference and Exhibit. Fort Lauderdale, FL, AIAA.

Coleman, H. and W. G. Steele Jr. (1999). Experimentation and Uncertainty Analysis for Engineers. Canada, John Wiley & Sons.

Dailey, C. L., J. L. Hieatt, et al. (1991). Nuclear Electric Propulsion Performance Maps for Planetary Missions. AIAA/NASA/OAI Conference on Advanced SEI Technologies, Cleveland, OH.

Foster, J. E., T. Haag, et al. (2004). The High Power Electric Propulsion (HiPEP) Ion Thruster. 40th AIAA/ASME/SAE/ASEE Joint Propulsion Conference and Exhibit, Fort Lauderdale, FL.

Goddard, R. H. (1960). The Green Notebooks. Clark University, Worchester, MA.

Goebel, D. M. and I. Katz (2008). Fundamentals of Electric Propulsion: Ion and Hall Thrusters. Pasadena, CA, Jet Propulsion Laboratory California Institute of Technology.

Group, P. P. (July 2004). Ion Beam Source Manual DC Filament Cathode/Filament Neutralizer Estes Park, CO, Plasma Process Group.

Haas, J. M., F. S. Gulczinski III, et al. (1998). Performance Characteristics of a 5 kW Laboratory Hall Thruster. AIAA/ASME/SAE/ASEE 34th Joint Propulsion Conference and Exhibit. Cleveland, OH, AIAA.

Hamley, J. A., J. McDowell, et al. (1998). "The Design and Perfromance Charcteristics of the NSTAR PPU and DCIU." AIAA.

Jahn, R. G. (1996). Physics of Electric Propulsion. New York, McGraw Hill, Inc.

Li, Z., C. W. Hawk, et al. (2005). Characterization of an 8-cm Diameter Ion Source System. 41st AIAA/ASME/ASEE Joint Propulsion Conference & Exhibit, Tuscon, AZ.

Li, Z., C. W. Hawk, et al. (2004). Plasma Jet Velocimetry By Cross-Correlation. 40th Joint Propulsion Conference.

Linnell, J. A. and A. D. Gallimore (2006). "Efficiency Analysis of a Hall Thruster Operating with Krypton and Xenon." Journal of Propulsion and Power **22**(6).

Martinez-Sanchez, M. and J. E. Pollard (1998). "Spacecraft Electric Propulsion - An Overview." Journal of Propulsion and Power **14**(5): 688-699.

Murphy, D. M. The Scarlet Solar Array: Technology Validation and Flight Results.

NASA. (2007). "Anatomy of an Ion Engine." Retrieved July 5, 2008, 2008.

Noca, M. (2001). "Next Generation Ion Engines: Mission Performances."

Oleson, S., L. Gefert, et al. (2002). Mission Advantages of NEXT: NASA's Evolutionary Xenon Thruster. 38th Joint Propulsion Conference and Exhibit, Indianapolis, IN.

Polk, J. E., R. Y. Kakuda, et al. (2000). In-Flight Performance of the NSTAR Ion Propulsion System on the Deep Space One Mission Pasadena, CA, Jet Propulsion Laboratory California Institute of Technology.

Polsgrove, T. (2006). CHEBTYOP Users Manual, NASA.

Polsgrove, T., L. Kos, et al. (2006). Comparison of Performance for New Low-Thrust Trajectory Tools. AIAA/AAS Astrodynamics Specialist Conference and Exhibit. Keystone, CO, AIAA.

Rawlin, V. K. (1995). Power Throttling the NSTAR Thruster. 31st AIAA/ASME/SAE/ASEE Joint Propulsion Conference and Exhibit, San Diego, CA.

Schuettpelz, B., Z. Li, et al. (9-12 July 2006). Plume Diagnostics Supporting Magnetic Nozzle Plasma Detachment Demonstration Experiment. 42nd AIAA/ASME/SAE/ASEE Joint Propulsion Conference & Exhibit. Sacremento, CA, AIAA.

Shimada, S., K. Sato, et al. (1987). 20-mN Class Xenon Ion Thruster for ETS-VI. AIAA-1987-1029, 19th International Electric Propulsion Conference, Colorado Springs, CO.

Sutton, G. P. and O. Biblarz (2001). Rocket Propulsion Elements. New York, NY, John Wiley & Sons, Inc.

Mel'kumov, T. M. (1964). Pioneers of Rocket Technology, Selected Works. Moscow, Academy of Sciences of the USSR, Institute for the History of Natural Science and Technology.